Aalborg Universitet

Experimental Study of the Development of Scour and Backfilling

Hartvig, Peres Akrawi; Thomsen, Jess Mccann; Frigaard, Peter; Andersen, Thomas Lykke

[Link to publication from Aalborg University](#)

Experimental study of the development of scour & backfilling[1]

Peres Akrawi Hartvig[2,3], Jess McCann Thomsen[4], Peter Frigaard[1], Thomas Lykke Andersen[1]

Abstract

This paper deals with the development of scour holes in time and space around individual offshore monopiles. It is based upon physical flume tests of a model-scale pile subjected to current and/or irregular water waves. The main focus is upon backfilling, i.e. the wave-induced or current-wave-induced deposition of sediment into holes that have been previously scoured. The development of the scour depth, scour volume and a so-called scour shape factor is quantified which may be useful for understanding and benchmarking the development of scour holes.

Keywords: Scour, backfilling, time scale, wave, offshore, foundation, pile.

1   Introduction

The offshore wind energy industry is supporting new research in the field of scour around offshore foundations. The goal is to predict the development of the scour holes in space and time. This is relevant when planning the deployment of conventional scour protection around the foundation. In addition, it is also crucial for considering partially or fully *unprotected* designs which may be both physically feasible and economically attractive at some wave-dominated locations.

The target field conditions are monopiles with diameters of 5-6.5 m in a sea state that is both wave-dominated and unsteady in the sense that the sea state parameters are statistical processes. The target bed consists of erosion-prone soil such as fine sand or non-cohesive silt that is typically in a live-bed condition, i.e. the entire bed is perpetually being transported by the flow.

The present knowledge on live-bed scour around piles mainly rests on physical model-scale tests. These include the studies by Sumer et al. [1992, 1992b, 1993] and Dey et al. [2006] for live-bed scour in steady current or linear regular water waves and by Sumer & Fredsøe [2001] for steady current, linear irregular waves and combined current and waves. Some of this pioneering work is recognized in the present DNV. However, some of this work – especially on the temporal development - is yet to be validated by others and under field-scale conditions.

Furthermore, there is a substantial lack of knowledge concerning the backfilling process around piles, i.e. the wave-induced or current-wave-induced deposition of sediment into holes that have been previously scoured. Sumer & Fredsøe [2001] focused only on the equilibrium properties of a backfilled bed during their current-wave tests. Fredsøe et al. [1992] treated both the temporal and equilibrium properties of backfilling, but this was in the context of pipelines.

The present paper attempts to address this knowledge gap on backfilling around monopiles. It presents spatial and temporal results of scour and backfilling based on physical model-scale tests. The monopile has been placed in well-sorted fine sand and subjected to alternating sequences of current and/or irregular water waves. During the tests, the bed surface near the pile has been measured by laser and these data are used for deriving measures to quantify the scour hole. The present results may be useful for understanding and benchmarking the development of scour holes.

The rest of the paper is organized as follows: Section 2 presents some of the above-mentioned studies in more detail. Sections 3 and 4 turn to the present tests and describe the test set-up and procedure. Section 5 introduces and discusses the flow and bed conditions. Section 6 presents the results on scour and backfilling, proposes models to describe these processes and compares the results with the existing studies of Section 2. The conclusion of the findings is given in Section 7.

2   Review of existing studies

In this section, the findings of existing studies are presented which will be refered to later on in the paper. Sumer et al. [1992, 1992b, 1993] and Dey et al. [2006] have examined live-bed scour for a vertical monopile in initially plane sand bed subjected to steady current or linear regular water waves. They suggested the following empirical relation for the scour depth development:

$$S = S_\infty \cdot \left(1 - e^{-t/t_s}\right) \tag{1}$$

where S is the actual scour depth at time t, S_∞ is the equilibrium scour depth and t_s is a characteristic time for the scour depth development. The empirical values of the equilibrium scour depths are:

$$
\begin{aligned}
\text{Steady current:} \quad & S_{\infty,c}/D = 1.3 \pm 0.7, \quad && \theta_{cr} < \theta \\
\text{Linear regular waves:} \quad & S_{\infty,w} = S_{\infty,c} \cdot \left(1 - e^{-0.03(K-6)}\right), \quad && \theta_{cr} < \theta, \quad 6 \le K
\end{aligned}
\tag{2}
$$

where $S_{\infty,c}, S_{\infty,w}$ are the equilibrium scour depths for current-only or wave-only flows, respectively, D is the pile diameter, K is the Keulegan-Carpenter number of the near-bed wave flow, θ is the actual Shields number and θ_{cr} is the critical Shields number corresponding to initiation of bed motion. The Shields number is defined as:

$$\theta \equiv \frac{U_f^2}{gd \cdot (s-1)} \tag{3}$$

where U_f is the bed friction velocity, $g = 9.81\,\text{N/kg}$ is the acceleration due to gravity, d is a characteristic grain size, $s = \rho_s/\rho_w$ is the relative grain-water density, ρ_w is the density of water and ρ_s is the density of the solid grains of the soil. The variables U_f, K are detailed later in this paper. The characteristic time for the scour depth development was cast into dimensionless form in the following way:

$$t_s = \frac{t_s^* \cdot D^2}{\sqrt{gd^3 \cdot (s-1)}} \tag{4}$$

where t_s^* is the normalized characteristic time. The latter is given by the following empirical relations:

Steady current:
$$t_s{}^* = \frac{\theta^{-2.2}\,\delta_c/D}{2000}, \quad 0.06 \leq \theta \leq 0.29, \quad 0.04 \leq \delta_c/D \leq 10, \quad 9\cdot10^3 < R_c < 1.3\cdot10^5$$

(5)

Linear regular waves:
$$t_s{}^* = \frac{\theta^{-3}K^3}{10^6}, \quad 0.07 \leq \theta \leq 0.19, \quad 7 \leq K \leq 34$$

where δ_c is the boundary layer thickness and R_c is the Reynolds number for current that are defined later. Sumer & Fredsøe [2001] have further examined live-bed scour in combined current and linear irregular waves. The initially plane beds have been scoured by steady current and subsequently backfilled when waves have been superimposed on the current. Based upon their data, the following empirical expression for the equilibrium scour depth has been suggested by Sumer & Fredsøe [2002, p.198]:

Current with linear irregular waves:
$$S_{\infty,cw} = S_{\infty,c} \cdot \left(1 - e^{-A\cdot(K-B)}\right), \quad \begin{array}{ll} A = 0.03 + 0.75 r_{cw}{}^{2.6}, & B = 6e^{-4.7r_{cw}} \\ \theta_{cr} < \theta & 4 \leq K \leq 26 \end{array}$$

(6)

where $S_{\infty,cw}$ is the equilibrium scour depth for the current-wave flow and r_{cw} is a current-wave velocity ratio. The latter is defined by:

$$r_{cw} = \frac{U_{c,D/2}}{U_{c,D/2} + U_{m0}}$$

(7)

where $U_{c,D/2}$ is the mean current velocity at the distance $D/2$ from the bed and U_{m0} is a characteristic velocity of the wave-induced flow near the bed as detailed later. Thus, the equilibrium backfilled hole in a current-wave flow may be much smaller than the initial current-scoured hole. No temporal expression in connection with (6) was presented.

3 Test set-up

Returning to the present physical model-scale tests, they have been conducted by the second author at the hydraulic laboratories of Aalborg University (AAU) in Denmark and Ghent University (GU) in Belgium. The tests have previously been reported in Thomsen [2006] but are published here in revised form. There are similarities in the set-up with the tests of Margheritini et al. [2006] and Vos [2008] that have been conducted concurrently. The set-ups are illustrated in Figure 1 and elaborated in this section.

The generic components of the flumes are pistons to generate water waves in one direction, a beach to absorb them downstream and reduce reflection and finally, a pump system that can operate in forward and reverse direction. In the set-up at GU, the flow that emanates from the inlet from the pump is guided into longitudinal direction before it mixes with the existing flow in contrast to the set-up at AAU. The centre region of the flume contains the equipment that is particular to the present tests and is detailed in the following:

- A *sand pit* with a *pile* is placed in its centre to simulate scour of an erodible bed. The pit is 4 m long and filled with sand with the estimated relative grain-water density $s = 2.65$. The sand is well-sorted and the grain diameter corresponding to the median percentile is $d_{50} = 0.15\,\text{mm}$ in the set-up at AAU and $d_{50} = 0.10\,\text{mm}$ at GU. These values are used for the characteristic grain size d in this paper. Concerning the risk of liquefaction for these grain sizes, a discussion is given in Section 5.5. The cylindrical pile has the diameter $D = 10\,\text{cm}$ and is composed of a floor-mounted bottom-piece (Figure 2) and a smooth removable upper-piece, co-supported at its top during the tests at GU.

- An *erosion profiler* measures the bed surface in the vicinity of the pile. The same kind of erosion profiler has been used at AAU and GU. The profiler consists of a downward-directed laser probe that is submerged into the water during operation and is mounted on a vehicle that can move in three dimensions and is supported along the flume walls. The profiler and its software EPro v. 1.2 have been developed by Meinert [2006] at AAU and been used in a few recent published tests, e.g. Jensen et al. [2006] and Margheritini et al. [2006].

- Three *wave gauges* measure the water surface elevation at multiple points and a *flowmeter* measures the streamwise velocity approximately mid-depth (the exact elevation for the velocity measurement has not been noted). In the set-up at AAU, the wave gauges and the flowmeter (Denshi Kogyo, type 'DS-102-XY', ultrasonic) are mounted upon a fixed frame 2 m upstream of the pile. The relative distance between the wave gauges is estimated to 10-20 cm. The sample frequency for the water surface elevation and velocity measurements is 25 Hz. In the set-up at GU, the flowmeter (Nautilus, electromagnetic) is mounted upon a fixed frame 2 m downstream of the pile. The wave gauges are mounted upon movable frames in a semi-circular fashion around the pile – one gauge directly upstream of the pile and the remaining two closer and parallel to the flume wall. Here, the sample frequency for the water surface elevation is 40 Hz and some of the gauge samples are unavailable, and all of the velocity samples are unavailable.

- A *video camera* is placed outside of the flume adjacent to the pile and directed towards the pile. Video recording has only been done occasionally during the set-up at GU. In addition, photos have occasionally been taken during the tests at AAU and GU.

- The *water depth* near the centre region is maintained at about $h = 0.3\,\text{m}$ during all tests. The tests have been performed with fresh water with an estimated density $\rho_w \approx 1000\,\text{kg}/\text{m}^3$ and estimated kinematic viscosity $\nu \approx 1.3 \cdot 10^{-6}\,\text{m}^2/\text{s}$.

In summary, the geometric scale between the model pile and a target field pile is 1:50-65. The corresponding geometric difference between the model and field sediment is much smaller. The set-up is regarded as a compromise between reducing scale effects while avoiding boundary effects from the flume walls. As shown in Figure 1, the flume is 10-12 times wider than the pile, which is considered sufficient for avoiding boundary effects when the bed is plane or scour holes are relatively small. However, when the scour holes are largest, the ratio between flume and scour width is reduced to about 2 and the flume walls are likely disturbing the flow and scour processes.

4   Test procedure

The test procedure is presented in this section. The following steps have been taken for each test series:

1) *Bed re-establishment:* At the beginning of a test series, eroded sand in the downstream direction of the pit is moved back into the pit and the pit is leveled manually by manpower. This process leads to some compaction of the initial bed. The corresponding void ratio has not been measured.

2) *Sand deposition:* Due to the lack of an upstream sand supply, the sand pit outside of the scour hole sunk during some test runs. In this paper, this phenomenon is termed *global erosion*. In order to reduce this effect, sand has been deposited in the upstream region of the pit occasionally in subsequent tests series (the exact test series and runs have not been noted). The correction for global erosion is discussed in Section 5.5 on bed conditions.

3) *Flow generation:* The generation of waves and/or current is initiated, as well as the data acquisition from the wave gauges and flowmeter.

4) *Flow pause and pile disassembly:* The flow generation and acquisition is paused (the flow durations are detailed later). The upper-piece of the pile is temporarily dismantled and at GU, the frames with wave gauges are temporarily dislocated along the flume. The process of dismantling and assembling the upper-piece is considered to have negligible influence on the bed profiles. The flume and pump system remains undrained and time is allowed for the water surface to become still. It has been observed that the suspended grains deposit quickly on the bed when the flow generation is paused. The bed profiles are not later adjusted for this deposition and will therefore vary from instantaneous measurements, assumingly with a couple of millimeters.

Bed profiling: The erosion profiler's laser probe is submerged into the water and travels above the bed along a square wave path (⎕⎕⎕) according to a targeted horizontal rectangular grid. The profiler automatically adjusts its vertical position to satisfy the working range of the laser while avoiding obstructions. The targeted horizontal grid spacing is 10 mm or 15 mm as detailed in

5) Table 1. The vertical inaccuracy of the laser is about $\pm 1\text{mm}$ according to prior tests in Vos [2008] and the profiled surfaces of the disassembled pile cap. The horizontal deviation from the targeted grid during the profiling is typically 0-3 mm but does reach about 20 mm in series A-B and about 60 mm in series C-E. The relatively high maximum deviation occurs systematically at few points near the downstream pile perimeter when the scour holes are relatively large. This is caused by the pile acting as an obstruction to the back-scattered laser light and at GU, also due the uneven pile cap. It is not reasonable to adjust these values by interpolation of the neighboring measurements since the profiled surface is discontinuous at the interface between the pile and the bed. The implications of the error for the estimation of the scour depth and scour volume are discussed in Section 5.5 on bed conditions.

6) *Pile re-assembly:* The upper-piece of the pile is re-installed. At GU, the pile is co-supported at its top and the frames with wave gauges are moved back into place.

7) Steps 2-6 are repeated for the remaining runs in the test series.

5   Flow and bed conditions

In this section, the measures for the flow and bed conditions are defined and discussed.

5.1   Current conditions

Current velocity: The undisturbed mean velocity of the current U_c is computed by time-averaging each velocity sample or if unavailable as in the current-wave tests, is taken as the reported value. Thus, the measure approximately represents the mean streamwise mid-depth velocity. The boundary layer for current is considered to be fully developed and its thickness is taken as identical to the water depth, i.e. $\delta_c = h$.

In the present tests, it is noted that low-frequent standing waves of considerable magnitude arise along the flume in connection with the abrupt pump initiation or termination. This is shown in Figure 3 at a dominant frequency of 0.05-0.07 Hz (period of 15-20 s) which appears to damp away after a couple of cycles. Due to these reasons, the mean velocity is considered to have an inherent uncertainty of $U_c \approx \pm 0.05\,m/s$ and for the shortest test runs lasting a minute, the stationary attribute of the current is considered to be weak. The stated value for the uncertainty is only indicative and serves to assert that the mean flow values are subjected to statistical uncertainty. A smoother pump initiation/termination may have been desirable but would not repudiate the difficulties in relating the actual transient flow to a steady flow and quantifying the effects of the initial and final flow conditions on the sensitive bed.

Turbulence level: The turbulence level is defined by:

$$I_T \equiv \frac{\sigma_u}{U_c} \tag{8}$$

where I_T is the turbulence level and σ_u is the standard deviation of a velocity sample. When excluding the time span of the above-mentioned standing waves, the undisturbed streamwise velocity samples at AAU typically have a turbulence level of 10 %.

Bed friction velocity: The undisturbed bed friction velocity corresponds to a plane (unrippled) undisturbed bed. In the current-only tests, this is computed by the Colebrook-White formula which is valid for laminar, transient or turbulent boundary layer flows in pipes and channels with steady mean current [Chadwick et al., 2004, pp.104,128]:

$$U_{fc} = U_c \cdot \sqrt{\frac{f_c}{2}}, \qquad f_c = \frac{f_d}{4}, \qquad \frac{1}{\sqrt{f_d}} = -2\log_{10}\left(\frac{k_N}{3.7D_e} + \frac{2.51}{R_e\sqrt{f_d}}\right), \qquad R_e = \frac{U_c D_e}{\nu} \tag{9}$$

where U_{fc} is the undisturbed mean bed friction velocity in steady current, f_c is the corresponding friction factor, f_d is the Darcy-Weisbach friction factor and $k_N = 2.5d$ is the equivalent Nikuradese bed roughness. Furthermore, $D_e = 4A_w/P_w$ is the equivalent pipe diameter for a flume where A_w is the wetted cross-sectional area and P_w is the wetted perimeter. The implicit relation (9) is solved iteratively for each test run, providing a friction factor in the range $f_c = 0.004 - 0.005$.

5.2   Wave conditions

Targeted wave characteristics: When generating waves, the pistons have been targeting irregular waves with the following JONSWAP spectrum: Significant wave height $H_{m0} = 0.12\,\mathrm{m}$, peak period $T_p = 1.64\,\mathrm{s}$ (peak frequency 0.6 Hz) and peak enhancement factor $\gamma = 3.3$.

Actual wave characteristics: The actual wave climate in the flume is *shallow* since the water depth is relatively small compared to the longest wave lengths. Therefore, the longest waves are interdependent and horizontally asymmetric. The latter is evident from the sampled water surface elevations that exhibit asymmetry about the mean as shown in Figure 4. In the following frequency-domain analyses of the wave climate and near-bed flow, the samples are by definition interpreted as Fourier series and therefore cannot properly address the non-linear attributes.

Conventional frequency-domain and time-domain analyses have been performed in WaveLab 3.11, developed by Andersen [2009] at AAU, all analyses without band-pass filter. The analyses reveal that the significant wave height H_{m0} of the frequency-domain and the significant wave height H_s of the time-domain, i.e. the mean of the 1/3-highest wave heights, are $\pm 0.02\,\mathrm{m}$ from the targeted value. Furthermore, the peak frequency is $\pm 0.1\,\mathrm{s}$ from the targeted value. In average, 10 minutes of wave action corresponds to about 400 wave cycles.

On a minor note, the shape of the actual wave spectrums deviate from one test run to another and also from the targeted spectrum. This deviation is expected due to the relatively short duration of the wave test runs and the shallow water condition. In the set-up at AAU, the measurements from the wave gauge array indicate that only minor wave reflection is present and they are therefore considered representative for the pile position too.

The maximum wave height from the time-domain analyses range from 0.18-0.21 m in the test runs. From the video recording, occasional wave breaking on the pile is observed. This is worth noting since wave breaking appears to enlarge equilibrium scour holes due to the increased turbulence level according to Carreiras et al. [2000]. From the video recordings, the concentration of suspended grains appears to increase during the passage of large or breaking waves.

For the wave-only runs, the wave lengths corresponding to the significant wave height are $\lambda \approx 2.5 - 2.7\,\mathrm{m}$ according to calculations based on linear and 5th order Stokes theory, respectively, both computed with the target peak period and a nil depth-averaged discharge. Since the pile width is relatively small compared to this wave length, i.e. $D/\lambda \approx 4\% < 20\%$, the pile is classified as slender and the effects of diffraction are not important according to Sumer & Fredsøe [2002].

Characteristics of near-bed flow: In Sumer & Fredsøe [2001], the following definition of the near-bed Keulegan-Carpenter number has been suggested for linear irregular waves:

$$K = \frac{U_{m0}T_p}{D} \tag{10}$$

where K is the near-bed Keulegan-Carpenter number , $U_{m0} = \sqrt{2 \int_0^\infty S_{uu}(f) df}$ is a near-bed characteristic velocity and S_{uu} is the variance spectral density of the near-bed velocity. For linear waves, the variance spectra of the streamwise velocity and the water surface elevation are linked by the following transfer function, see e.g. Frigaard & Hald [2004]:

$$\frac{S_{uu}}{S_{\eta\eta}} = \left(\omega \frac{\cosh(k(z+h))}{\sinh(kh)} \right)^2 \tag{11}$$

where $S_{\eta\eta}$ is the variance spectral density of the water surface elevation, z is the upward elevation from the mean water surface, $\omega = 2\pi/T = 2\pi f$ is the wave circular frequency, T is the wave period, f is the wave frequency, $k = 2\pi/\lambda$ is the wave number and λ is the wave length. The circular frequency satisfies the dispersion equation for linear water waves, see e.g. Frigaard & Hald [2004]:

$$\omega^2 = gk \tanh(kh) \tag{12}$$

The streamwise bed velocity, i.e. $z = -h$, is considered as an appropriate measure for the near-bed velocity whereas it is nil in reality due to the no-slip condition.

A minor numerical benchmark test has been performed for the wave test runs at AAU when both velocity and elevation samples have been available. The variance spectra of the actual velocities and those estimated by (10)-(12) with temporarily $z \approx -h/2$ have been compared. The spectra generally differ in shape, but nevertheless lead to characteristic velocities that only vary by about ± 0.02m/s within each test run. In addition, a comparison has been performed for regular waves according to 5th order and linear wave theory as described earlier. The ratio of the maximum streamwise bed velocity below the wave crest according to the former and latter approach, respectively, is $0.274/0.258 = 1.06$, implying only a minor increase of the Keulegan-Carpenter number due to non-linearity of the wave.

Therefore, the Keulegan-Carpenter number is computed by (10) without any adjustment for non-linearity. The measure is derived from the wave-induced velocity alone even in combined current-wave flows to allow comparison with existing studies. This provides $K = 3$ in all wave test runs. Since wave-induced scour is observed in test run D.02 (Table 5), this value of the Keulegan-Carpenter number is considered to be sufficiently large to induce vortex shedding at the pile's lee-side near the bed. This is not unreasonable since scour has been observed by Sumer & Fredsøe [2001] for $K \approx 4$ for a circular pile in irregular linear waves. In contrast, vortex shedding and scour for a circular pile in *regular* linear waves occurs only for $K \geq 6$ according to Sumer et al. [1993].

Bed friction velocity: In the wave-only test runs, the bed friction velocity is based on Stokes' theory for oscillatory flows with laminar boundary layers over plane beds as given by Fredsøe & Deigaard [1992, pp.19,30,33]:

$$U_{fw} = U_{m0} \cdot \sqrt{\frac{f_w}{2}}, \qquad f_w = \frac{2}{\sqrt{R_a}}, \qquad a = \frac{U_{m0} T_p}{2\pi}, \qquad R_a = \frac{U_{m0} a}{\nu} < 5 \cdot 10^5, \qquad \delta_w = \sqrt{\frac{\nu T_p}{\pi}} \tag{13}$$

where U_{fw} is the undisturbed maximum bed friction velocity in waves, f_w is the corresponding friction factor, δ_w is the corresponding boundary layer thickness, R_a is the amplitude Reynolds number and a is the streamwise bed stroke of the wave motion. In the wave-only runs, the amplitude Reynolds numbers is $R_a \approx 5 \cdot 10^3 - 8 \cdot 10^3$, the relative roughness is $a/k_N \approx 140 - 180$, the boundary layer thickness is $\delta_w = 0.8\text{mm}$ and the friction factor is $f_w \approx 0.02 - 0.03$.

5.3 Current-wave conditions

Bed friction velocity: The bed friction velocity for the current-wave runs is based on the method of Fredsøe [1984] which assumes the following piece-wise mean velocity profile and a fully rough bed:

$$u_{cw}(z) = \begin{cases} \dfrac{U_{fcw1}}{\kappa} \cdot \ln\left(\dfrac{z}{k_{cw}/30}\right), & \delta_m \leq z \\[3mm] \dfrac{U_{fcw0}}{\kappa} \cdot \ln\left(\dfrac{z}{k_N/30}\right), & k_N/30 < z < \delta_m \end{cases} \tag{14}$$

where u_{cw} is the mean velocity at elevation z from the theoretical bed, δ_m is the corresponding thickness of the wave boundary layer, k_{cw} is the apparent roughness acting on the flow outside the wave boundary layer and $\kappa = 0.4$ is Kármán's constant. U_{fcw1} and U_{fcw0} are the mean bed friction velocities for the flow outside and inside the wave boundary layer, respectively, where the latter is used for the computation of the Shields number. In the wave-current tests, the coefficients are obtained numerically as $a/k_N \approx 160$, $U_{m0}/U_{fcw0} \approx 13 - 24$, $U_{m0}/U_{fcw1} \approx 11 - 14$, $k_{cw}/k_N \approx 2 - 8$ and $\delta_m/k_N < 7$.

Current-wave ratio: When computing the current-wave ratio, (14) is used to estimate $U_{c,D/2} = u_{cw}(D/2)$ which provides a current-wave ratio of $r_{cw} \approx 0.5 - 0.6$ for the current-wave runs.

5.4 Common flow conditions

Flow duration: In all test runs, the nominal duration of the flow is taken as the time between initiation and pause of the flow generators (piston and/or pump). When this information is unavailable from the measurements, the duration is taken as the reported value if available. The resulting flow durations are 1 minute to 2 hours for the current-only runs, 10 minutes for the wave-only runs and 10 minutes to 2 hours for the current-wave runs.

Reynolds numbers: Finally, the following Reynolds numbers for the current-only and wave-only runs are calculated based on pile diameter:

$$R_c = \frac{U_c D}{\nu}, \qquad R_w = \frac{U_{m0} D}{\nu} \tag{15}$$

where R_c, R_w are Reynolds numbers, both having the order of magnitude 10^4.

5.5 Bed conditions

In this section, the measures for the bed conditions are discussed. They are all based upon the bed surface measurements of the erosion profiler. The coordinate system for all bed representations in the paper is shown in Figure 5 where the *z*-axis is horizontal and directed towards the flume end region. Except for the tests with tidal current as detailed later, the end region coincides with the downstream direction. In addition to the scour depth, this section will introduce two additional parameters: the scour volume and the scour shape factor. These provide additional information about the scour process and also appear to be indispensable for quantifying the backfilling process which doesn't appear to be sufficiently described by the scour depth alone as discussed in Section 6.2.3.

Bed forms: By judgment of the longitudinal bed profile relatively far from the pile, the wave length and height of the bed forms is roughly estimated.

Global erosion: The magnitude of global erosion during each test run has been estimated by calculating the average bed elevation along the upstream and longitudinal borders of the bed grid, i.e. furthest from the pile. Subsequently, the corresponding bed profile is lifted by a constant value that is equal the global erosion, resulting in an *adjusted* bed profile. Global erosion has only occurred for some of the runs in series A where the original profile has typically been lifted by 1-3 cm as detailed in Table 2. Besides impairing the derived bed properties, this may also have influenced the flow itself.

Scour depth: The scour depth *S* is derived from the adjusted bed profile and is calculated as the average of the bed elevation at points that lie around the pile base, but at some distance to it, as shown in Figure 5. These points are termed *contour points* and comprise between 20 and 32 points. This approach is considered to be more reliable than only using the inner-most points where the bed elevation appears to be slightly deeper (see e.g. test run A.08 in Figure 8 where the apparently deepest bed elevation is 10.7 cm but $S = 9.9\,\text{cm}$) but is more error-prone due to higher horizontal deviation from the targeted grid and possible vertical repositioning of the laser. Whether the bed elevation at the inner-most points is deeper remains unsettled since alternative and accurate bed measurements along the pile perimeter are unavailable. The horizontal location of the contour points is fixed throughout a test series even when the location and size of the profiled pile differ slightly. Once global erosion occurs, the precision of the scour depth is reduced from $\pm 1\,\text{mm}$ up to $\pm 3\,\text{cm}$.

Scour volume: The calculation of the scour volume *V* is derived in four steps. First, the bed elevations at all points that are enclosed by the contour points are temporarily set equal to *S*. Secondly, the horizontal extent of the scour hole is estimated by an ellipsis whose center and dimensions typically vary with each test run. Then, the void volume between the initial $(t = 0)$ and adjusted bed surface within the elliptic domain is calculated by numerical integration. Finally, the scour volume *V* is determined as the difference between the void volume and the pile volume where the latter is calculated as $V_{pile} = SD^2\pi/4$. By neglecting the profiled pile in the first step and introducing its volume in the last step, the reliability of the scour volume estimate is increased greatly. This is especially true in the test runs at GU where the surface of the pile cap is uneven.

This approach leads to a scour volume that encompasses all voids that exist within the elliptic domain. This includes those formed by ripples and multiple areas of bed lowering during early-stage scour, and also includes the possible influence of deposition downstream. However, ripples are considered to have negligible influence on the scour volume since they, on average, cancel out if they are present within the elliptic domain. In series B-D, the elliptic domain covers the entire measured bed. In series A-B, the longitudinal dimension of the ellipsis is between 14-47 cm, corresponding to about 2-7 ripple wave lengths for wave runs and 1-4 ripple wave lengths for current runs where the measured ripple wave lengths are given in Tables 2-3.

The scour volume is sensitive to global erosion and is considered to have an inaccuracy of as much as $\pm 0.002 \text{m}^3$ (2 liters) for the large scour holes with considerable global erosion. For comparison, the sensitivity of the scour volume depends with 1-2 orders of magnitude less upon the ellipsis definition and with about an additional order of magnitude less upon the choice of method for numerical integration.

Scour shape factor: Based upon the scour depth and scour volume, a dimensionless variable is derived which is termed the *scour shape factor* ψ and relates the scour volume and scour depth according to the following definition:

$$V \equiv \psi\, S^3 \tag{16}$$

It is emphasized that the definition in (16) is valid for any three-dimensional void (or body) and thus the scour shape factor has been computed for all the present tests except for those where the scour volume has not been derived. However, once the gross features of a scour hole resemble a hemisphere or cone, the scour shape factor allows a further geometric interpretation: In these cases, the scour shape factor is related to the angle of the slope of the void. This can be seen from the following geometric relationship:

$$\psi = \frac{c}{\tan^2 \varphi} \tag{17}$$

where c is a variable that depends upon the shape of the void, being $c = \pi/3$ for an axisymmetrical cone or $c = 2\pi/3$ for an axisymmetrical hemisphere, and φ is the slope angle. Some examples of the correspondence between the scour shape factor and the slope of different axisymmetrical cones are given in Figure 6. It is noted that the scour shape factors of two voids of arbitrary shape are identical if they are geometrically *similar*, i.e. scaled uniformly in all dimensions.

In the present tests, the scour holes are generally asymmetrical about the lateral axis with upstream and downstream parts that have distinct volumes, shapes and slope angles. A decomposition of the scour shape factor into its upstream and downstream parts is not presented, although this would furnish a direct agreement between the slope angle in (17) and the observed one for each part for conical scour holes. The inaccuracy of the scour shape factor is inversely proportional to the scour depth to the third power and thus ranges from about ± 1 for the large scour holes to about ± 50 for the smallest scour holes.

Influence of liquefaction: The risk of liquefaction during the wave-only or wave-current runs has not been investigated experimentally in connection with the present tests and is assessed here with reference to the studies of Sumer et al. [2006, 2007]. They examined liquefaction of beds with grain sizes $d_{50} = 0.060$mm or $d_{50} = 0.147$mm. The bed was artificially installed in a loose state and subjected to regular waves with a period of 1.6s and wave heights $H = 0.05$m $-$ 0.175m in a water depth of 0.42m. Liquefaction occurred for the fine grain size when $H \geq 0.102$m and did not occur at all for the coarse grain size which can be attributed to the higher hydraulic conductivity of the soil with the coarse grain size. The present tests have comparable wave conditions and the difference in water depth is disregarded as it is considered to have negligible influence on the effective stresses in the soil. The authors are not aware of studies that support the hypothesis that backfilled sediment deposits in a loose fashion corresponding to the artificial installation described above. On the contrary, the backfilled sediment may be born into a medium-dense or dense state by the vibrating action of flow agents and would in this case be resistant to liquefaction under the corresponding stress conditions. On these grounds, the wave tests at AAU are considered to be resistant to liquefaction. The wave and wave-current tests at GU may have undergone liquefaction if the backfilled sediment deposits loosely but as mentioned above, this condition may not be satisfied naturally.

Concerning the possible influence of liquefaction, Sumer et al. [2006] found that liquefaction began in the upper bed layer with the smallest internal friction and led to compaction of the underlying soil layer until it eventually covered the entire depth and the liquefaction process had finished. A compaction process may still occur without liquefaction during weaker wave conditions but leads to comparably less compaction. Sumer et al. [2007] found a significant increase of the scour depth around piles when the seabed had undergone a process of liquefaction and compaction.

Validity of time scale estimation: Finally, the present tests have not fully investigated the equilibrium states of the scoured or backfilled holes. This introduces uncertainty on the estimates of the equilibrium bed – but will this also affect the estimates of the temporal properties since these are generally coupled? This is discussed in the following passages whereas the actual values are presented in the next section. The discussion takes its point of departure in the scour *volume* development formula (25) as introduced later, but could equivalently be based on the similar scour *depth* development formula (1) and would have the same implications. The discussion begins by assuming (25) to be valid for scour and backfilling and proceeds with examining its differential equation:

$$\frac{dV}{dt} = \frac{V_\infty - V}{t_V} = \frac{V_\infty}{t_V} - \frac{V}{t_V} \tag{18}$$

When the scour process is far from an equilibrium state, the last term on the rhs. of (18) is negligible:

$$\frac{dV}{dt} \approx \frac{V_\infty}{t_V}, \quad V \ll V_\infty, \qquad \text{scour far from equilbrium} \tag{19}$$

It can be seen from (19) that when given data far from equilibrium, the time scale and equilibrium scour volume are indeterminate, only their ratio V_∞/t_V can be estimated. In contrast, when given data not too far from equilibrium, the two terms on the rhs. of (18) are of comparable orders of magnitude and thus the time scale and the equilibrium value can be demarcated. Among the present scour tests, runs A.01-02 and perhaps also runs A.05-08 as detailed in the following section are susceptible of being far from equilibrium. For these, the temporal and equilibrium properties are assumed to be identical to test runs A.11-14 which appear to be close to an equilibrium state. This equivalence is considered to be a reasonable approximation since the test conditions are similar except for the configuration of the initial bed and some variation in the Shields number.

A similar analysis can be performed for backfilling processes and this leads to a different and less challenging asymptotic behavior. In this case, the *first* term on the rhs. of (18) is negligible:

$$\frac{dV}{dt} \approx -\frac{V}{t_V} \quad , \quad V_\infty \ll V, \qquad \text{backfilling far from equilbrium} \tag{20}$$

The implication of (20) is that the time scale is independent of the equilibrium scour volume for backfilling processes far from equilibrium. Thus, the time scale of backfilling processes in this state should not be questioned on the account of an uncertain equilibrium value. This is the case for the backfilling runs A.14-17 and A.20-23 as introduced shortly. For the remaining backfilling runs that are closer to equilibrium, any uncertainty in the time scale may be balanced by an improved estimate of the equilibrium value. On a final note, all of the backfilling runs that belong to the same series are assumed to have identical temporal and equilibrium properties. This is considered to be a good approximation in light of their practically identical test conditions and effectively extends the data range used for calibration.

Curve fitting procedure: The developments of the scour depth, scour volume and scour shape factor have been fitted to differential and integrated equations in the following section and a brief description of the procedure for obtaining the fitted values and their 84% confidence intervals is given here. The fitted parameters are determined by the method of non-linear least squares which minimizes the sum of squared residuals along the response-axis:

$$\min_{\theta_1,\theta_2}\left(R = \sum_{i=1}^{n}\left(y_i - y_{i,predicted}\right)^2 \right), \qquad y_{i,predicted} = y_{i,predicted}\left(x_i,\theta_1,\theta_2\right) \tag{21}$$

where R is the sum of squared residuals, $\left(x_i,y_i\right)$ is the ith measured data pair, $y_{i,predicted}$ is the corresponding predicted response, n is the number of data pairs and θ_1,θ_2 are the two fitting parameters of the equation. The optimization has been performed on the integrated equations, namely (25), (29) and (33), rather than their differential equations since the latter would entail a quality loss when transforming the data points with large gradients into finite differences. Assuming the residuals to be approximately normal distributed, the 84% confidence interval of the mean of each fitting parameter is computed by:

$$\theta_p \in \left[\hat{\theta}_p \pm \sigma_{\theta_p} F_T^{-1}\left(n_{dof},\alpha\right)\right], \quad \alpha = \left(1-0.84\right)/2, \quad n_{dof} = n-2, \quad p = 1,2 \tag{22}$$

where θ_p is the unknown true mean of the *p*th fitting parameter, $\hat{\theta}_p$ is its sample mean as obtained from (21), σ_{θ_p} is its sample standard deviation and F_T^{-1} is the α-percentile in the Student's T-distribution with n_{dof} degrees of freedom. The standard deviations of the parameters are estimated by:

$$\mathbf{C} = \begin{bmatrix} \sigma_{\theta_1}{}^2 & C_{12} \\ C_{21} & \sigma_{\theta_2}{}^2 \end{bmatrix} = \sigma_r^2 \cdot \mathbf{N}^{-1}, \qquad \sigma_r^2 = \frac{R}{n_{dof}}, \qquad \mathbf{N} = \mathbf{J}^T\mathbf{W}\mathbf{J}, \qquad \mathbf{J}^T = \begin{bmatrix} \partial y_1/\partial\theta_1 & \partial y_2/\partial\theta_1 & \cdots & \partial y_n/\partial\theta_1 \\ \partial y_1/\partial\theta_2 & \partial y_2/\partial\theta_2 & \cdots & \partial y_n/\partial\theta_2 \end{bmatrix} \qquad (23)$$

where $\mathbf{C}$ is the variance-covariance matrix of the mean of the fitting parameters, σ_r is the standard deviation of the residuals and $\mathbf{N}$, $\mathbf{W}$ and $\mathbf{J}$ are the normal, weight and Jacobian matrices, respectively, where *T* denotes transpose. The off-diagonal components of the weight matrix are zero and the diagonal components are given by the weight of each data pair. The weights and the components of the Jacobian matrix are detailed later. Unless otherwise stated, uniform weights have been used which implies that the weight matrix is equal to the identity matrix.

6   Results & discussion

Having now reviewed the test assumptions, the results are presented in this section. Based upon the results, empirical expressions for the scour volume and scour shape factor are suggested since these variables are linked to the scour depth by (16). The results are also compared with a generalized version of the conventional scour development formula (1) of Sumer et al. [1992b].

Five test series have been conducted. An overview is given in

Table 1 and the tests are detailed in Tables 2-6. In series A and C-E, the current is directed towards the flume's end region (denoted by ←), while series B also introduces a current in the reverse direction (→) to resemble tidal conditions. Series A-B are classified as live-bed tests due to the emergence of bed forms relatively far from the pile in the sampled bed profiles. For series C-E, the extent of the bed grid is typically too small to allow an accurate determination of the bed forms, scour volume or the scour shape factor. Photos reveal that series C is in a clear-water state, i.e. global erosion is nil, and series D-E are in live-bed states as shown in Figure 7. The computed undisturbed Shields number $\theta \approx 0.01$ for some of the current-wave runs in series E may be dubious since it is much below the critical Shields number θ_{cr} in previous empirical studies [Soulsby, 1997, p.106] and yet, the regular ripples in Figure 7 support that live-bed has occurred during the wave-current runs. For series D-E, global erosion is likely nil too since the corresponding scour depths are relatively small and the mean velocities are only somewhat greater than those of series C.

6.1 Scour development

The clear-water current scour from an initially plane bed is given by series C. The video recording reveals that almost immediately after initiation of the current, a horseshoe-formed hole emerges directly in front of the pile as well as two holes laterally and slightly upstream of the pile. After about an hour (model-scale), the holes merge. In this series, the estimated undisturbed Shields number is $\theta \approx 0.05$. This is slightly below the critical Shields number θ_{cr} in previous empirical studies [Soulsby, 1997, p.106] and thus agrees with the visual observation of erosion only in the vicinity of the pile.

Live-bed current scour from an initially wave-scoured bed is shown in Figure 8 with detailed cross-sectional bed profiles in Figure 9 and Figure 10. These runs belong to series A and have an estimated Shields number of $\theta \approx 0.2$. Here, a considerable scour hole develops after a few minutes (model-scale) and sand is deposited downstream of the scour hole. Bed ripples arrange in an irregular pattern with ripple lengths of 10-20 cm.

Once the scour hole has developed along the entire pile perimeter, the angle of the upstream slope of the scour hole remains nearly constant. The physical reason is likely that the slope reaches and remains in a nearly continuous state of sliding failure. As pointed out by Roulund et al. [2005, Section 3.2], this could be due to excavation of the base of the scour hole by the horseshoe vortices and/or drag and gravity forces from incoming ripples at the top of the scour hole. The angle of the *downstream* slope of the scour hole varies slightly more. By studying the profiled upstream slopes of all the current-induced scour holes, the upstream repose angle has been computed to $\varphi_r = 32°$ in all cases despite the difference in grain size between the tests at AAU and GU.

6.1.1 Scour shape factor development

The development of the scour shape factor during the scour tests is shown in Figure 11. The scour shape factor is shown as a function of the scour volume, but could equivalently be interpreted as a function of the scour depth or the plane extent of the scour holes. It is clearly seen that as the scour volume increases, the scour shape factor converges towards a minimum value, equal to 8-9 in the present tests.

This corresponds to the relatively fast convergence of the slope angles towards the repose angles. Once the scour shape factor has converged, the rate of scour depth is only affected by the rate of scour volume which can be deduced from (16) and can be seen in Figure 12. This effect is also observed in the data of Link & Zanke [2004] and Link [2006, p.52] where the scour volume and scour depth has been monitored during clear-water and live-bed scour tests.

6.1.2 Scour volume development

The development of the scour depth and scour volume is shown in Figure 12. For series A and B.01-07, it is seen that the scour volume rate decreases in magnitude with increasing time or increasing initial scour volume. This empirical behavior may be captured by the following ordinary 1st order linear differential equation:

$$\frac{dV}{dt} = \frac{V_\infty - V}{t_v}, \quad t_v > 0 \tag{24}$$

where V_∞ and t_v are constant with respect to time and are interpreted as the scour volume at the equilibrium state and a characteristic time for the *scour volume* development, respectively. Equation (24) has the solution:

$$V = V_\infty + (V_0 - V_\infty) \cdot e^{-t/t_v} \tag{25}$$

where V_0 is the initial scour volume at $t = 0$. The Jacobian components of (25) are:

$$\mathbf{J}_i^T = \begin{bmatrix} \partial V_i / \partial V_\infty \\ \partial V_i / \partial t_v \end{bmatrix} = \begin{bmatrix} 1 - e^{-t_i/t_v} \\ (V_{0,i} - V_\infty) e^{-t_i/t_v} \cdot t_i / t_v^2 \end{bmatrix}, \quad i = 1, 2, \ldots, n \tag{26}$$

The characteristic time t_v could be a function of the local Shields number and for wave flows, also of the Keulegan-Carpenter number. Similarly to (4), t_v is cast into a dimensionless form to allow comparisons between different configurations:

$$t_v = \frac{t_v^* \cdot D^2}{\sqrt{gd^3 \cdot (s-1)}} \tag{27}$$

where t_v^* is the normalized characteristic time for the scour volume development. The time scale t_v for the scour *volume* is generally different from the corresponding time scale t_s for the scour *depth*.

Equation (25) has been fitted to the present test data by the method outlined in Section 5.5 and with the initial scour volumes specified as identical or close to the measured values. The measurements for series B are taken from the first tidal cycle. As shown in Figure 13, a good agreement between measured and predicted values is obtained with the following fitting parameters:

$$\left. \begin{array}{l} V_{0,A.01-02}/D^3 = 0 \\ V_{0,A.05-08}/D^3 = 0.9 \\ V_{0,A.11-14}/D^3 = 6.8 \end{array} \right\} \quad V_{\infty,A}/D^3 = 15.6 \pm 0.9, \quad t_{v,A} = 8.6\,\text{min} \pm 1.2\,\text{min}, \quad t_{v,A}^* = 0.38 \pm 0.05, \quad n = 10 \tag{28}$$

$$V_{0,B.01-07}/D^3 = 0, \quad V_{\infty,B.01-07}/D^3 = 3.1 \pm 0.1, \quad t_{v,B} = 6.9\,\text{min} \pm 0.6\,\text{min}, \quad t_{v,B}^* = 0.31 \pm 0.03, \quad n = 7$$

The values for the characteristic time t_v in (28) are relatively similar for test series A and B which is attributed to the similar test conditions. Curiously, scour in series B is slightly faster than in series A although the former is subjected to slightly weaker current, but this discrepancy is within the confidence range of the parameters.

6.1.3 Scour depth development

In order to compare the agreement with the conventional scour formula, (1) is generalized to allow a non-zero initial scour depth:

$$S = S_\infty + \left(S_0 - S_\infty\right) \cdot e^{-t/t_s}, \quad t_s > 0 \tag{29}$$

where S_0 is the initial scour depth. It is noted that (1) and (29) are identical when $S_0 = 0$ and both are based on the same differential equation. The Jacobian components of (29) are – similarly to (26) – given by:

$$\mathbf{J}_i^T = \begin{bmatrix} \partial S_i / \partial S_\infty \\ \partial S_i / \partial t_s \end{bmatrix} = \begin{bmatrix} 1 - e^{-t_i/t_s} \\ \left(S_{0,i} - S_\infty\right) e^{-t_i/t_s} \cdot t_i / t_s^2 \end{bmatrix}, \quad i = 1, 2, \ldots, n \tag{30}$$

A fair fit between the measurements from series A and B and (29) is obtained with the following set of parameters as shown in Figure 14:

$$\left. \begin{array}{l} S_{0,A.01-02}/D = 0 \\ S_{0,A.05-08}/D = 0.2 \\ S_{0,A.11-14}/D = 0.64 \end{array} \right\} \quad S_{\infty,A}/D = 1.23 \pm 0.1, \quad t_{S,A} = 4.6 \text{ min} \pm 1.3 \text{ min}, \quad t_{S,A}* = 0.20 \pm 0.06, \quad n = 10 \tag{31}$$

$$S_{0,B.01-07}/D = 0, \quad S_{\infty,B.01-07}/D = 0.57 \pm 0.03, \quad t_{S,B} = 4.0 \text{ min} \pm 0.6 \text{ min}, \quad t_{S,B}* = 0.18 \pm 0.03, \quad n = 7$$

The success of (29) in describing scour processes rests on the brief initial influence of the scour shape factor. Far from equilibrium, the scour volume increases much and the scour shape factor decreases much which both dictate a corresponding strong increase of the scour depth. The effect of the scour shape factor quickly diminishes hereafter and the scour volume development dictates the rest of the development which decays exponential according to both (25) and (29). It is noted that the scour depth during scour can be predicted more accurately by combining (16), (25) (or its corresponding differential equation) and the scour shape factor development in Figure 11. A mathematical expression for the latter has not been presented.

When applying the time scale formula (5) with $\delta_c/D = 3$ and $\theta \approx 0.1 - 0.2$ for series A and $\theta \approx 0.1$ for series B, the present values for t_S* in (31) lie within the range of the predicted values, thus supporting the time scale formula.

6.2 Backfilling development

The backfilling development from an initially current-scoured bed in series A is shown in Figure 15-Figure 17. After about half an hour (model-scale time) or about 1200 cycles of wave action, the scour hole is reduced significantly. Bed ripples organize in a regular pattern with fronts that are perpendicular to the water wave direction and with lengths of about 6 cm. The undisturbed Shields number is $\theta \approx 0.2$. In contrast to the scour tests, the bed ripples during the wave-only or current-wave runs extend down into the scour hole.

6.2.1 Scour shape factor development

During backfilling, the scour shape factor increases as the normalized scour volume decreases as shown in Figure 18. This suggests that the deposition of backfill is slightly concentrated at the base of the pile as implied by (17). The bed profiles further reveal that the backfill is slightly concentrated at the *lateral* regions of the pile as shown in Figure 17. The empirical development of the scour shape factor can be captured by the following ordinary 1st order non-linear differential equation:

$$\frac{d\psi}{d\left(V/D^3\right)} = -c_1 \cdot \left(V/D^3\right)^{-c_2} \tag{32}$$

where c_1, c_2 are dimensionless variables which are constant with respect to time in these test runs and considered to be functions of at least the sediment fall velocity, the Keulegan-Carpenter number and the near-bed velocity of superimposed current, if present. The solution to (32) is:

$$\psi = \psi_0 + \frac{c_1}{c_2 - 1} \cdot \left(\left(\frac{V}{D^3}\right)^{1-c_2} - \left(\frac{V_0}{D^3}\right)^{1-c_2} \right), \quad c_2 \neq 1 \tag{33}$$

The Jacobian components of (33) are:

$$\mathbf{J}_i^T = \begin{bmatrix} \dfrac{\partial \psi_i}{\partial c_1} \\[2mm] \dfrac{\partial \psi_i}{\partial c_2} \end{bmatrix} = \begin{bmatrix} \dfrac{1}{c_2 - 1} \cdot \left(\left(\dfrac{V_i}{D^3}\right)^{1-c_2} - \left(\dfrac{V_{0,i}}{D^3}\right)^{1-c_2} \right) \\[4mm] \dfrac{c_1}{c_2 - 1} \cdot \left\{ \left(\dfrac{1}{c_2-1} + \ln\left(\dfrac{V_{0,i}}{D^3}\right) \right) \cdot \left(\dfrac{V_{0,i}}{D^3}\right)^{1-c_2} - \left(\dfrac{1}{c_2-1} + \ln\left(\dfrac{V_i}{D^3}\right) \right) \cdot \left(\dfrac{V_i}{D^3}\right)^{1-c_2} \right\} \end{bmatrix}, \quad i = 1, 2, \ldots, n \tag{34}$$

Since the variance of the scour shape factor seems to increase with decreasing scour volume, the scour shape factor measurements have been fitted with different weights for each sub series. Each weight has been determined in a precursor procedure by fitting its $n=4$ measurements to (33) and computing the weight as $w = 1/\sigma_r^2$ as suggested by (23). Figure 18 shows a good agreement between the measured and predicted scour shape factors with the following set of fitting parameters where the initial scour shape factors and scour volumes have been specified as identical to the measured ones:

$$\left. \begin{array}{lll} \psi_{0,A.02-05} = 17, & V_{0,A.02-05}/D^3 = 2.6, & w_{A.02-05} = 0.4 \\ \psi_{0,A.08-11} = 9, & V_{0,A.08-11}/D^3 = 9.1, & w_{A.08-11} = 4.5 \\ \psi_{0,A.14-17} = 9, & V_{0,A.14-17}/D^3 = 15.0, & w_{A.14-17} = 24.1 \end{array} \right\} \quad c_1 = 364 \pm 48, \quad c_2 = 2.0 \pm 0.1, \quad n = 12 \tag{35}$$

6.2.2 Scour volume development

The development of the scour depth and scour volume is shown in Figure 19 and the scour volume is shown separately in Figure 20. There is a fair agreement between the measurements of series A and equation (25), although there appears to be some systematic deviation for the smallest backfilled holes (A.02-05). The following fitting parameters have been used:

$$\left. \begin{array}{l} V_{0,A.02-05}/D^3 = 2.2 \\ V_{0,A.08-11}/D^3 = 9.1 \\ V_{0,A.14-17}/D^3 = 15.3 \end{array} \right\} \quad V_\infty/D^3 = 0.1 \left[0;1.4\right], \quad t_V = 88\,\text{min} \pm 13\,\text{min}, \quad t_V* = 3.9 \pm 0.6, \quad n = 12 \tag{36}$$

By comparison of the normalized characteristic times t_V* in (28) and (36), which are both live-bed cases, it can be seen that the scour in series A and B is about 10 times faster than backfilling in series A. Roughly speaking, the normalized time scale is $t_V* \approx 10^{-1}$ in the current-scoured tests and $t_V* \approx 10^0 - 10^1$ in the wave-backfilled tests.

For series D-E, only the scour depth has been derived. For the wave-current runs of series E, the scour volume has been estimated in the following three steps. First, the scour shape factor has been assumed to follow the development of (33) and by further use of (16), this implicitly determines the discrete values of the scour volume V_i:

$$V_i = \left(\psi_0 + \frac{c_1}{c_2 - 1} \cdot \left(\left(\frac{V_i}{D^3} \right)^{1-c_2} - \left(\frac{\psi_0 S_0^{\,3}}{D^3} \right)^{1-c_2} \right) \right) \cdot S_i^{\,3}, \quad i = 1, 2, \ldots, n \tag{37}$$

where S_0 and S_i are the initial and ith discrete measurement of the scour depth, respectively. Equation (37) is solved iteratively for a given set of c_1, c_2. Secondly, the resulting scour volumes have been fitted to the scour volume development formula (25). Lastly, the c_1, c_2 parameters that provide the best fit are chosen. As shown in Figure 20 for series E, a good fit is obtained based on the fitting parameters given below (without confidence intervals). The initial scour depths have been specified as identical to the measured ones and the initial scour shape factors correspond approximately to the initial slopes of the longitudinal profiles:

$$\left. \begin{array}{l} \psi_{0,E.02-05} = 9, \quad S_{0,E.02-05} / D = 0.73 \\ \psi_{0,E.06-10} = 10, \quad S_{0,E.06-10} / D = 0.88 \end{array} \right\} \quad c_1 = 29.4, \quad c_2 = 1.4, \quad \frac{V_\infty}{D^3} = 2.7, \quad t_V = 42 \text{ min}, \quad t_V{}^* = 1, \quad n = 11 \tag{38}$$

By comparison of the normalized characteristic times $t_V{}^*$ in (28), (36) and (38), it appears that wave-current-backfilling in series E is about three times slower than current-scour in series A-B and about four times faster than the wave-backfilling in series A. This supports the view that backfilling is generally slower than scour and indicates that the superposition of current upon waves accelerates the backfilling process compared to waves only. Furthermore, comparing the c_1, c_2 parameters in (35) and (38) suggests that the growth of the scour shape factor is much smaller in series E than in series A. The results for series E are only suggestive in light of its lack of scour volume measurements. Based upon the results of this section, the development of scour and backfilling is schematized in Figure 21.

6.2.3 Scour depth development

The backfilling test results in Figure 19 reveal that for holes that are initially small (e.g. A.02-05), the scour depth decreases much initially while the scour volume decreases little initially. For holes that are initially large (e.g. A.14-17), the scour depth decreases little initially while the scour volume decreases much. The generalized scour depth formula (29) agrees poorly with this behavior and is therefore not considered to be suited for predicting backfilling processes. It simply fails to account for the increasing influence of the scour shape factor. When the backfilled hole approaches equilibrium, the scour shape factor increases much and dictates a strong decrease of the scour depth despite the fact that the overall volume of the hole is nearly the same. In contrast, a good agreement can be obtained by the combined use of (16), (25) and (33) or their corresponding differential equations but the empirical parameters of these equations are limited to the present test conditions.

In Fredsøe et al. [1992], a comparative study was presented between the equilibrium wave-scoured bed and the equilibrium wave-backfilled bed in the context of pipelines. It was found that the scour depths of the two cases agreed quite well. This has not been the focus of the present tests but it may be noted that the wave scour runs D.01-02 reaches $S/D = 0.04$ whereas the backfilling runs A.02-05 reaches $S/D = 0.18$. The difference in values can be attributed to the lack of equilibrium of the former run. This is supported by the evidence of scour laterally to the pile but not longitudinally in the bed profile of D.02 (not shown).

Turning to the equilibrium scour depth of the current-wave runs, a fair agreement is found between series E and (6) with the following parameters where the current-only equilibrium scour depth has been estimated:

$$\left. \begin{array}{c} S_{\infty,c} \approx 9-10\,\text{cm} \\ r_{cw} \approx 0.5-0.6 \\ K=3 \end{array} \right\} \Rightarrow \quad A \approx 0.2, \quad B = 0.3-0.4, \quad S_{\infty,cw} \approx 3-5\,\text{cm} \tag{39}$$

7 Conclusion

In conclusion, this paper has presented physical model-scale flume tests for a cylindrical pile with diameter $D = 0.1\,\text{m}$ in well-sorted fine sand. The pile has been subjected to alternating sequences of current with and without superimposed irregular waves in a water depth of $h = 0.3\,\text{m}$. The flow generation has been temporarily paused during the tests and the pile disassembled, allowing profiling of the bed surface around the pile by laser. Thereby, bed surface snapshots for certain instances in time are obtained and bed properties are derived, such as the scour depth S, the scour volume V and a so-called scour shape factor $\psi = V/S^3$.

The velocity of the current is measured approximately mid-depth with a flowmeter and its mean value is $U_c = 0.2-0.5\,\text{m/s}$. The waves are irregular, non-linear and occasionally breaking on the pile. The undisturbed near-bed wave-flow is characterized by a Keulegan-Carpenter number $K = 3$ which is considered to be associated with lee-side vortex shedding.

The tests reveal that initially plane or wave-backfilled beds, when subjected to current, are scoured relatively quickly and obtain shapes similar to hemiellipsoids or cones. Both the scour volume rate and the scour depth rate decay exponentially during scour. A generalized version of the conventional scour depth development formula of Sumer et al. [1992b] provides a fair fit to the test results.

The tests further reveal that initially current-scoured beds, when subjected to waves, are backfilled about 10 times slower than the scoured ones. During backfilling, the scour volume rate decays exponentially. The backfill is slightly concentrated at the lateral region near the pile and this considerably affects the shape of the scour hole and the scour depth development, obscuring the use of the above-mentioned formula for backfilling processes. In contrast, this effect can be properly modeled by estimating the development of the scour volume and the scour shape factor as described in the paper.

Finally, some of the present test runs are impaired by one or more of the following uncertainties: Few or short test runs, uncertain flow information, influence of standing waves and global erosion as detailed in the paper. The proposed results are therefore only indicative and require future validation under the present and more general conditions.

8 Bibliography

Andersen, T.L., 2009. *WaveLab 3 Home*. [Online]. Available at: *http://hydrosoft.civil.aau.dk/wavelab* [Accessed 16 Mar 2009].

Carreiras, J., Larroudé, P., Santos, F.J.S. & Mory, M., 2000. Wave scour around piles. In *Proc. 27th International Conference on Coastal Eng. (ICCE)*. Sydney, 2000. Vol. 2.

Chadwick, A.J., Morfett, J.C. & Borthwick, M., 2004. *Hydraulics in civil and environmental engineering*. 4th ed. Taylor & Francis. ISBN 0415306086, 9780415306089.

Dey, S., Sumer, B.M. & Fredsøe, J., 2006. Control of scour at vertical circular piles under waves and current. *J. Hydraulic Eng.*, 132(3), pp.270-79. DOI 10.1061/(ASCE)0733-9429(2006)132:3(270).

Fredsøe, J., 1984. Turbulent boundary layer in wave-current motion. *J. Hydraulic Eng.*, 110(8), pp.1103-20. DOI 10.1061/(ASCE)0733-9429(1984)110:8(1103).

Fredsøe, J. & Deigaard, R., 1992. *Mechanics of coastal sediment transport*. Singapore: World Scientific Publishing Co. Ote. Ltd. ISBN 981-02-0840-5.

Fredsøe, J., Sumer, B.M. & Arnskov, M.M., 1992. Time scale for wave/current scour below pipelines. *International J. Offshore and Polar Eng.*, 2(1), pp.13-17. ISSN 1053-5381.

Frigaard, P. & Hald, T., 2004. *Notes for course in wave hydraulics*. 2nd ed. Aalborg University, Institute for Water, Soil and Enviromental Engineering.

Jensen, M.S. et al., 2006. *Offshore wind turbines situated in areas with strong currents*. Report. Offshore Center Danmark.

Link, O., 2006. *Untersuchung der Kolkung an einem schlanken zylindrischen Pheiler in sandigem Boden*. PhD thesis. Institut für Wasserbau und Wasserwirtschaft, Technische Universität Darmstadt. Heft 136. ISBN 3-936146-15-2.

Link, O. & Zanke, U., 2004. On the time-dependent scour-hole volume evolution at a circular pier in uniform coarse sand. In *Proc. 2nd International Conference on Scour and Erosion (ICSE)*. Singapore, 2004.

Margheritini, L., Martinelli, L., Lamberti, A. & Frigaard, P., 2006. Scour around monopile foundation for off-shore wind turbine in presence of steady and tidal currents. In Smith, J.M. ed. *Proc. 30th International Conference on Coastal Eng. (ICCE)*. San Diego, 2006. Vol. 3. World Scientific Publishing Co. Pte. Ltd.: Singapore. ISBN-13 978-981-270-991-2.

Meinert, P., 2006. EPro Non-contact erosion profiling: Brief overview. *Hydraulics and Coastal Engineering*, (40). ISSN 1603-9874, Available at: http://vbn.aau.dk/research/epro_noncontact_erosion_profiling(4268731).

Roulund, A., Sumer, B.M., Fredsøe, J. & Michelsen, J., 2005. Numerical and experimental investigation of flow and scour around a circular pile. *J. Fluid Mechanics*, Vol. 534, pp.351-401. DOI 10.1017/S0022112005004507.

Soulsby, R., 1997. *Dynamics of marine sands - A manual for practial applications*. London: Thomas Telford Publications. ISBN 0-7277-2584-X.

Sumer, B.M., Christiansen, N. & Fredsøe, J., 1992b. Time scale of scour around a vertical pile. In *Proc. 2nd International Offshore and Polar Eng. Conference*. San Francisco, 1992b. Vol. 3. ISBN 1-880653-03-6.

Sumer, B.M., Christiansen, N. & Fredsøe, J., 1993. Influence of cross section on wave scour around piles. *J. Waterway, Port, Coastal and Ocean Eng.*, 119(5), pp.477-95. ISSN 0733-950X/93/0005-0477.

Sumer, B.M. & Fredsøe, J., 2001. Scour around pile in combined waves and current. *J. Hydraulic Eng.*, 127(5), pp.403-11. ISSN 0733-9429/01/0005-0403-0411.

Sumer, B.M. & Fredsøe, J., 2002. *The mechanics of scour in the marine environment*. Singapore: World Scientific Publishing Co. Pte. Ltd. Reprinted 2005. ISBN 981-02-4930-6.

Sumer, B.M., Fredsøe, J. & Christiansen, N., 1992. Scour around vertical pile in waves. *J. Waterway, Port, Coastal and Ocean Eng.*, 118(1), pp.15-31. ISSN 0733-950X/92/0001-0015.

Sumer, B.M., Hatipoglu, F. & Fredsøe, J., 2007. Wave scour around a pile in sand, medium dense, and dense silt. *J. Waterway, Port, Coastal and Ocean Eng.*, 133(1), pp.14-27. DOI 10.1061/(ASCE)0733-950X(2007)133:1(14).

Sumer, B.M., Hatipoglu, F., Fredsøe, J. & Sumer, S.K., 2006. The sequence of sediment behaviour during wave-induced liquefaction. *Sedimentology*, 53(3), pp.611-29. DOI 10.1111/j.1365-3091.2006.00763.x.

Thomsen, J.M., 2006. *Scour in a marine environment*. MSc thesis. Aalborg University. Available at: http://projekter.aau.dk/projekter/research/scour_in_a_marine_environment(14765329).

Vos, L.D., 2008. *Engineering the influence of an offshore wind turbine on local flow conditions: Optimization of scour protection design for monopiles and quantification of wave run-up*. PhD thesis. Department of Civil Engineering, Ghent University.

Hydraulic Laboratory, Aalborg University, Aalborg
21.7 m long, 1.2 m wide, 1.5 m deep

EP: Erosion profiler
WG: Wave gauge
FM: Flowmeter
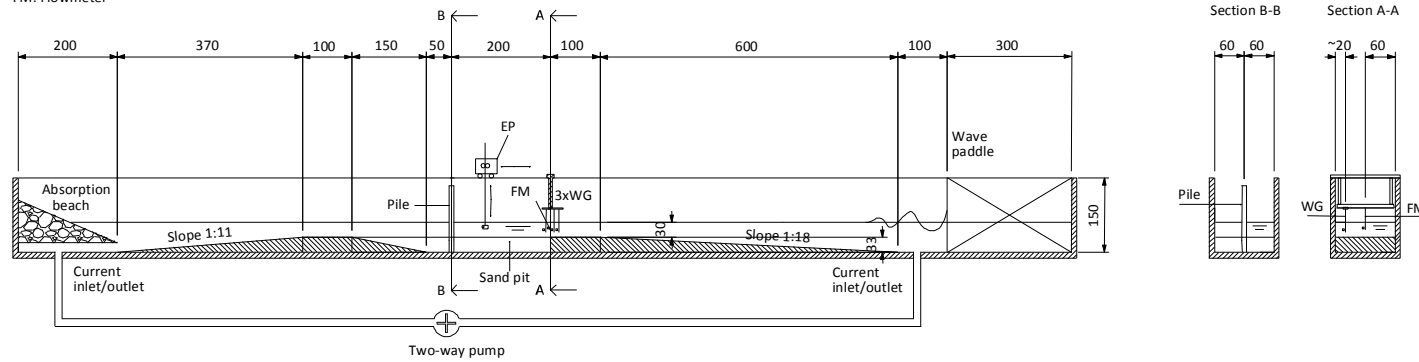
Hydraulic Laboratory, Ghent University, Ghent
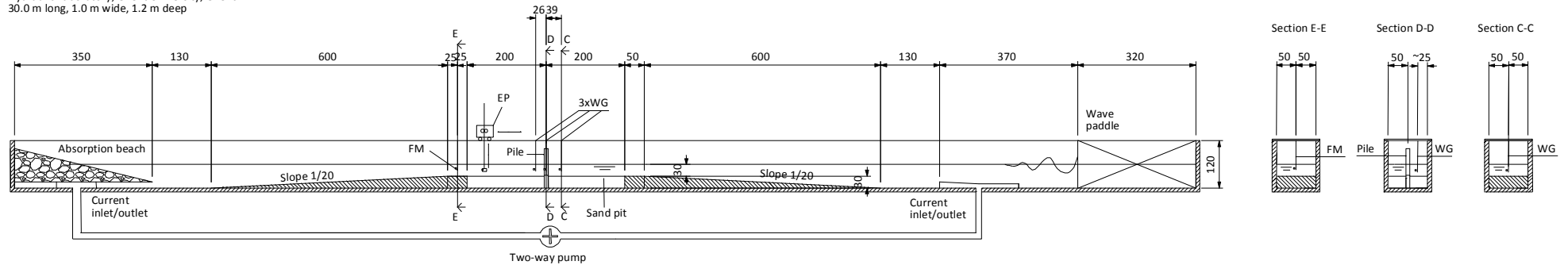30.0 m long, 1.0 m wide, 1.2 m deep

Figure 1: Test set-ups. All dimensions in cm.

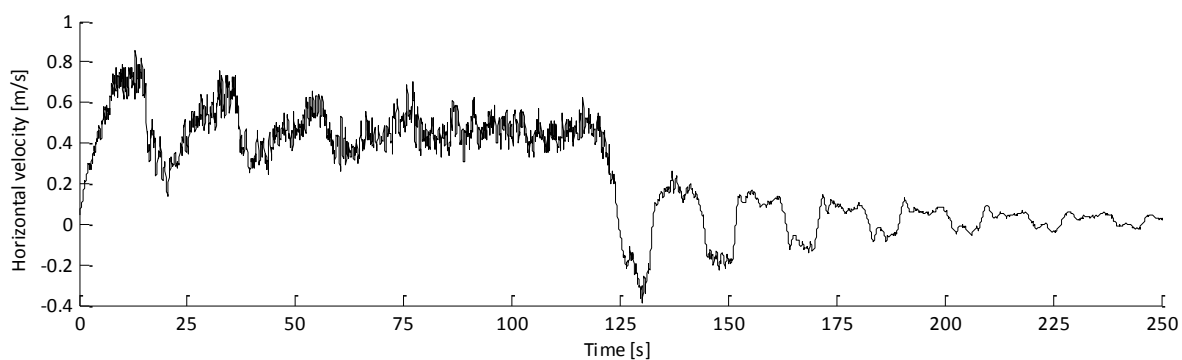*Figure 2: Disassembled piles at AAU (left) and GU (right).*

Figure 3: Measured streamwise velocity. Test run A.08 (Current) with a nominal duration of 120 seconds.
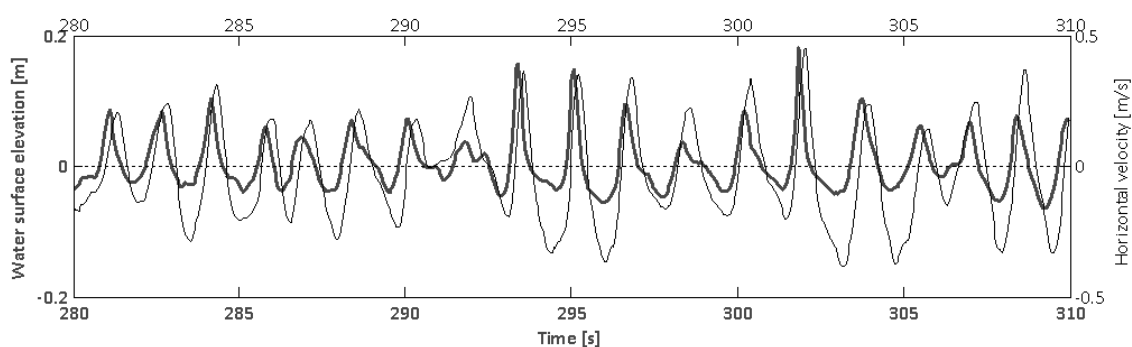*The pump is initiated at $t = 0$ and terminated at $t \approx 120\,\mathrm{s}$.*

Figure 4: Measured water surface elevation (bold curve) and streamwise velocity. Test run A.03 (Waves), entire duration is not shown.
Notice the asymmetric wave components of the water surface elevation due to the relatively shallow water depth in the flume.

- Bed elevation measurement

○ Bed elevation measurement ('contour point' for computing S)

···· Pile perimeter
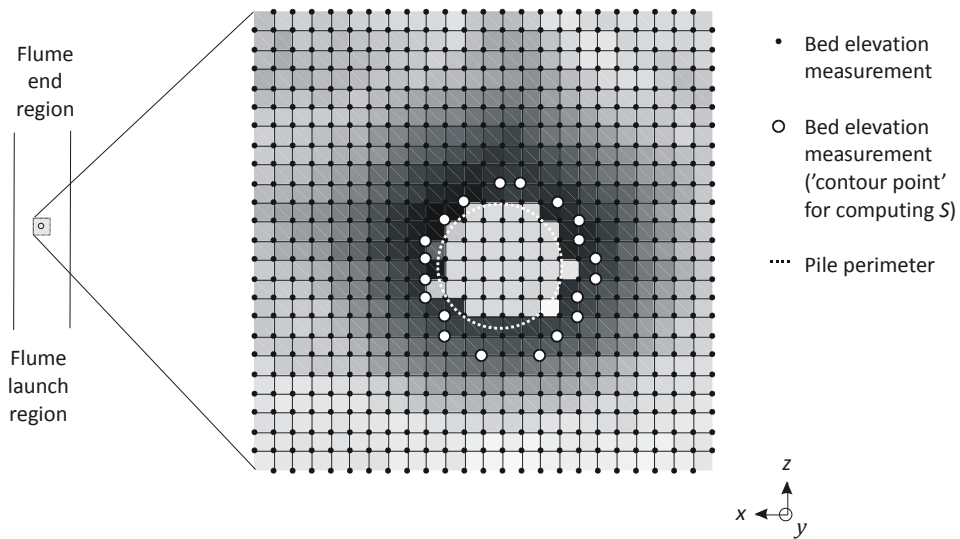
Figure 5: Bed elevation grid in test run A.02 (Current). Entire grid is not shown. Darker colors signify lower bed elevation.

Scour volume
$V = \psi S^3$

Scour depth S

Constant slope, ψ is constant

ψ_1 ψ_1 ψ_1

Changing slope, ψ varies

ψ_1 $\psi_2 > \psi_1$ $\psi_3 > \psi_2$
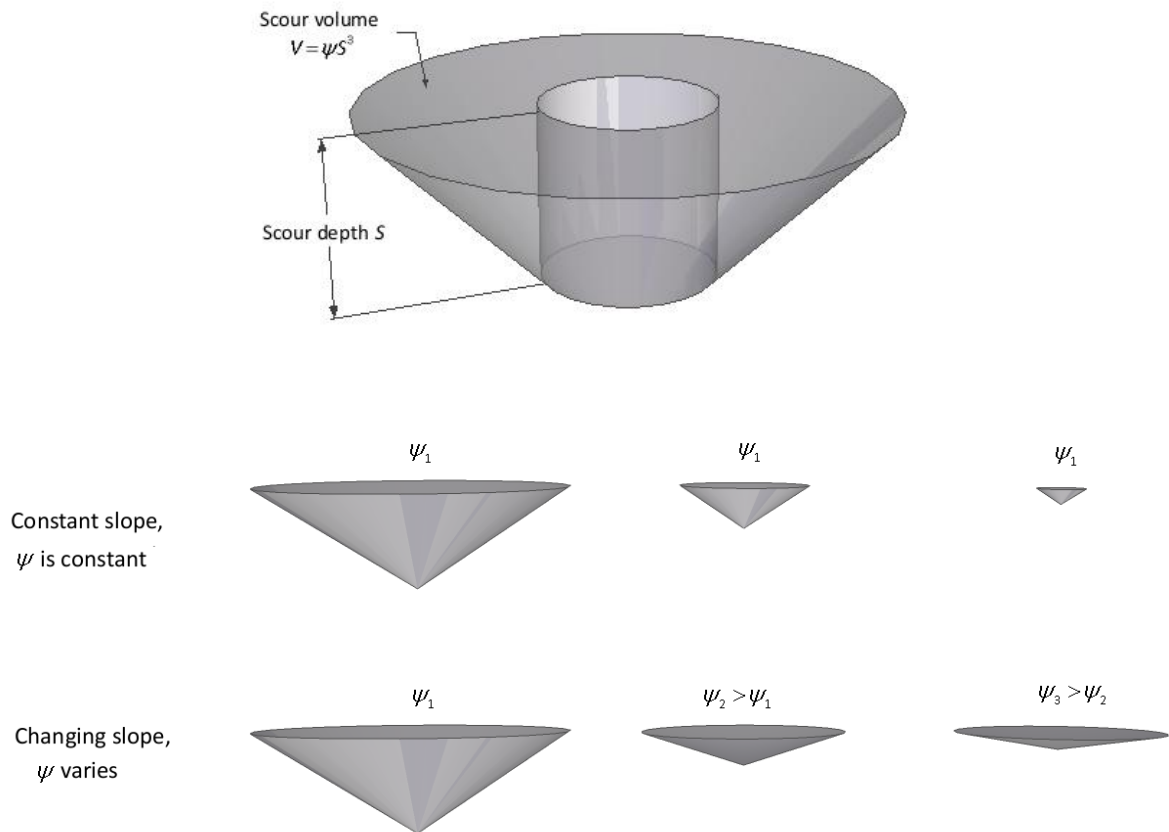
Figure 6: Correspondence between scour shape factor ψ and the slope of axisymmetrical cones.

Table 1: Test series overview.

| Series	Flow condition	Bed condition	Bed grid Length x Width, Spacing	Grain size d_{50} [mm]	Lab.
A	Current or irregular waves	Live-bed scour or backfilling	1.09 m x 0.80 m, 1.5 cm	0.15	AAU
B	Bidirectional current	Live-bed scour			
C	Current	Clear-water scour	0.30 m x 0.30 m, 1.0 cm	0.10	GU
D	Current or irregular waves	Live-bed scour or backfilling			
E	Current with irregular waves	Live-bed scour or backfilling			
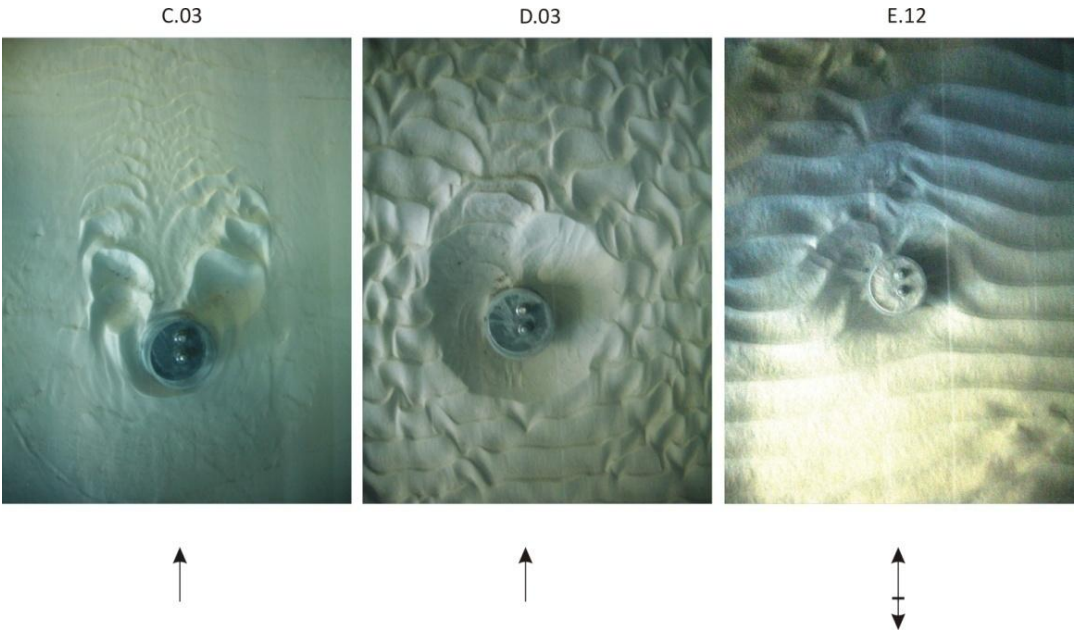
Figure 7: Photos of bed surfaces in series C-E. Single or double-head arrows indicate current or current-wave direction, respectively.

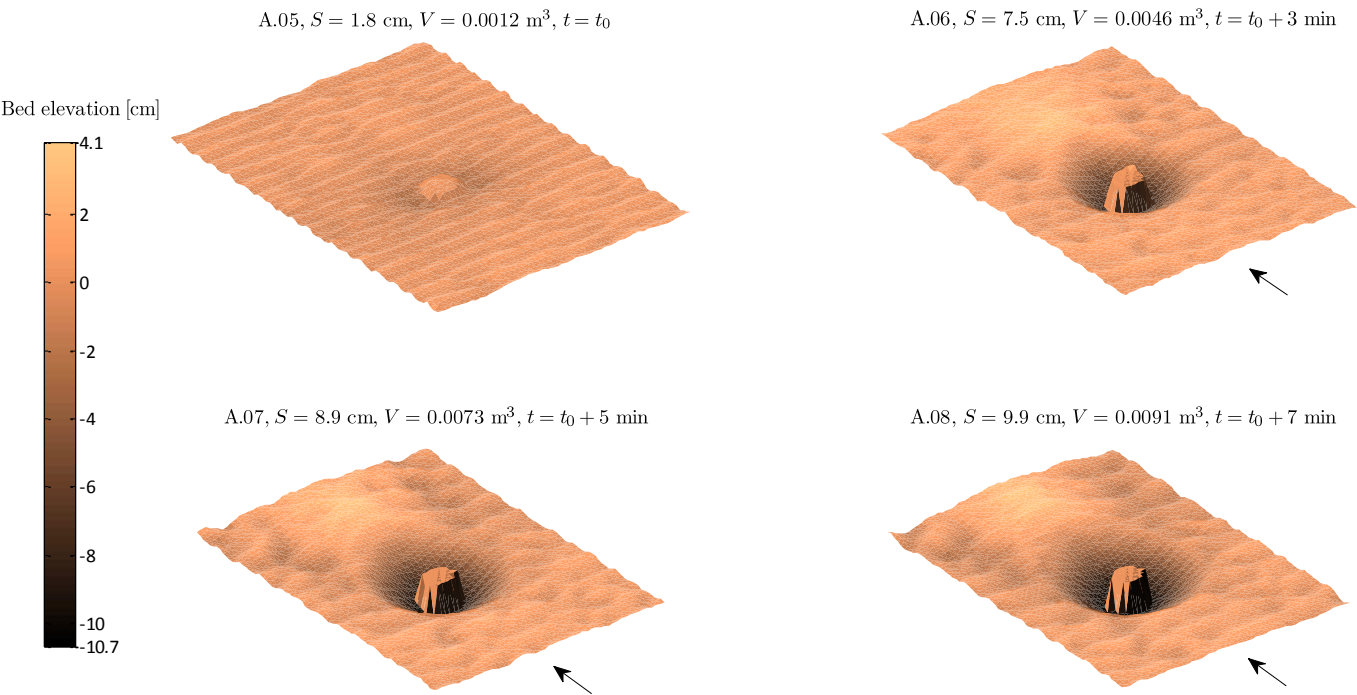*Figure 8: Bed surface development. Live-bed scour tests A.05-08 (Current) with undisturbed Shields number $\theta \approx 0.2$. Arrows indicate current direction.*
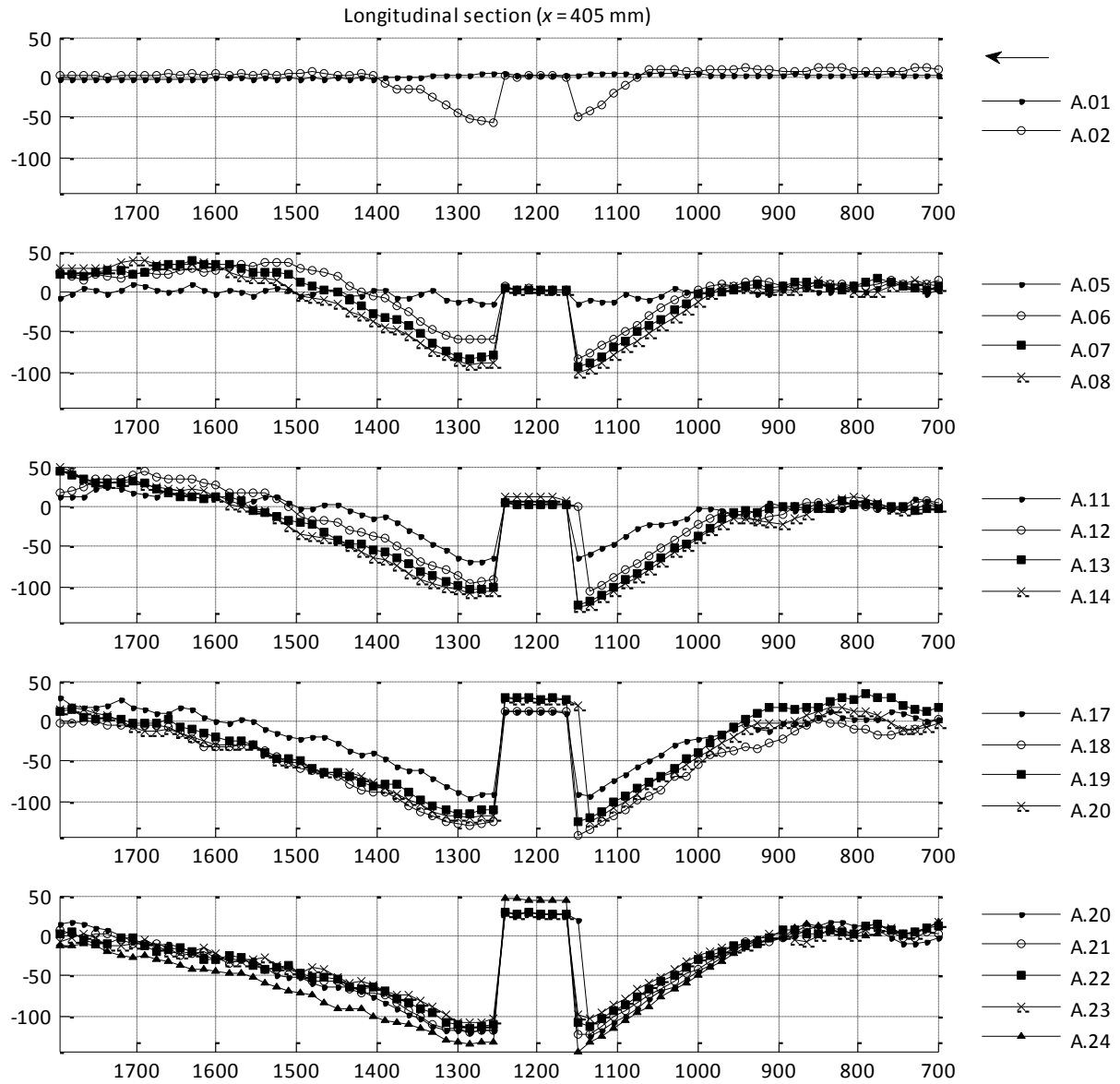
Figure 9: Longitudinal sections. Current sequences. Series A. Bed elevation and longitudinal axis z in mm.

Lateral section (z = 1210 mm)
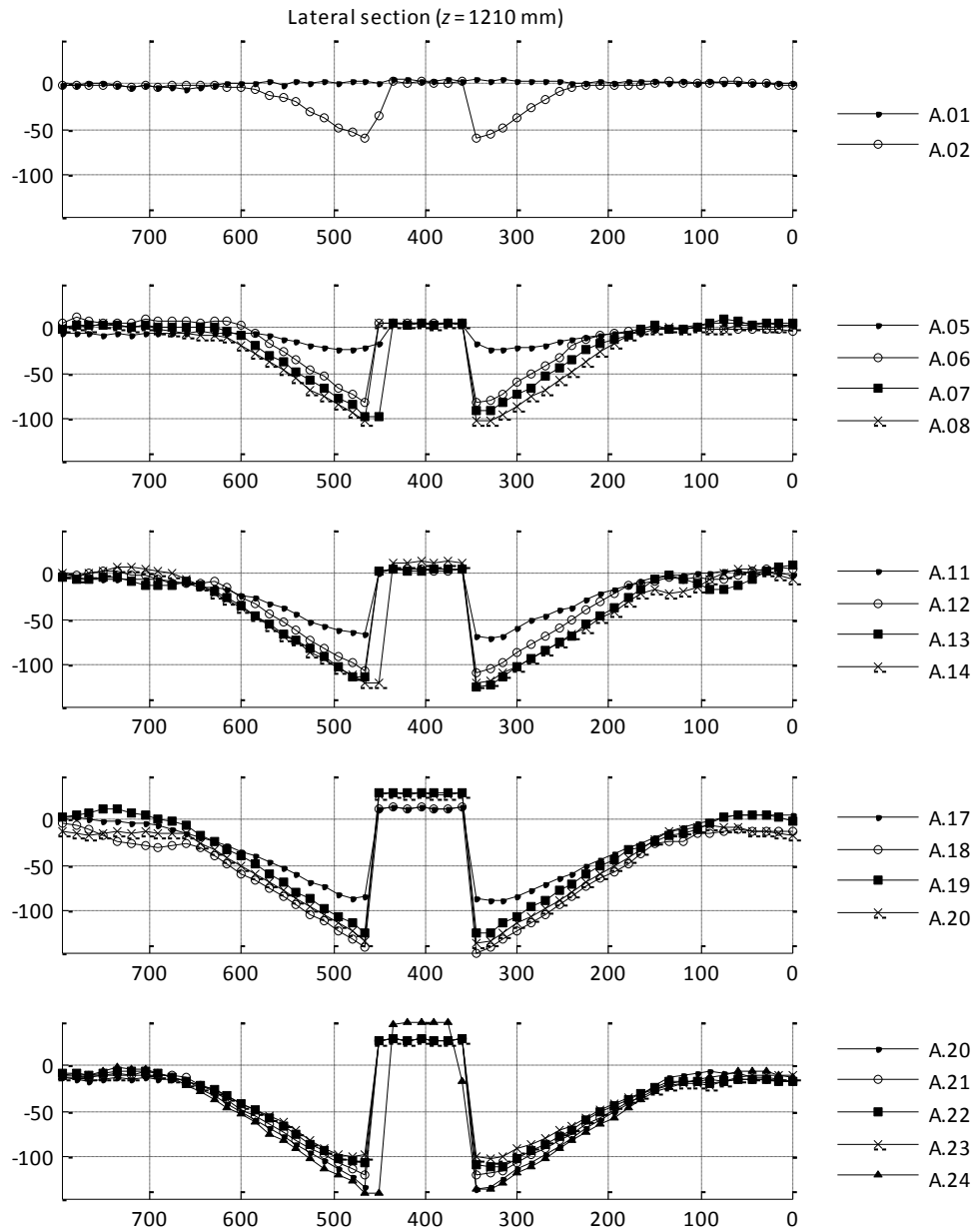
Figure 10: Lateral sections. Current sequences. Series A. Bed elevation and lateral axis x in mm.
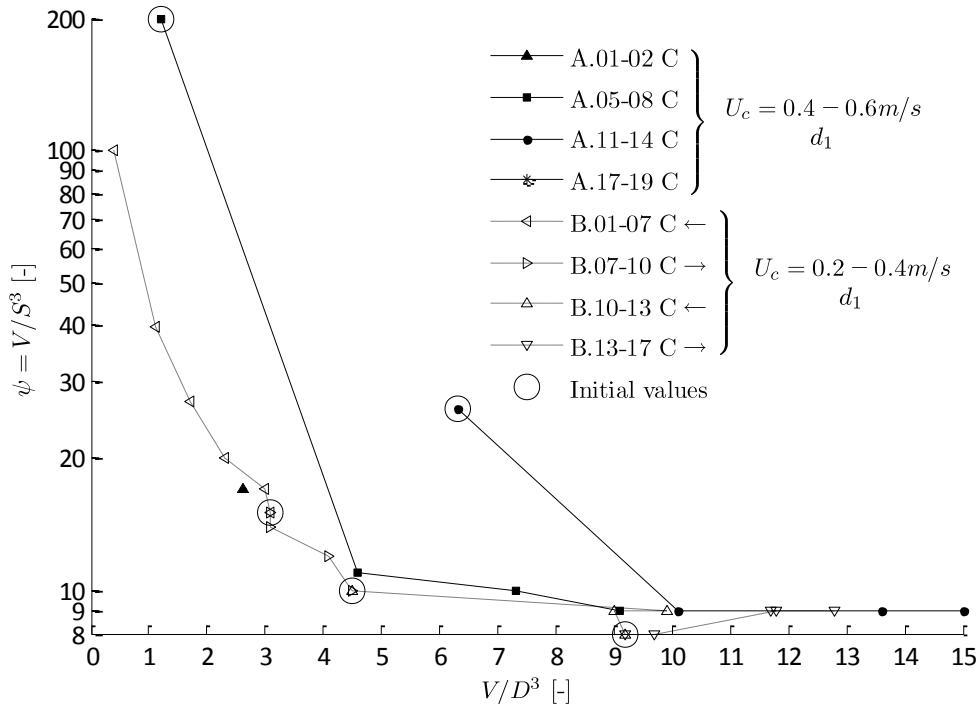
Figure 11: Measured scour shape factor and normalized scour volume. Scour tests.
Current-only (C) flows and grain size $d_1 = 0.15\text{mm}$.
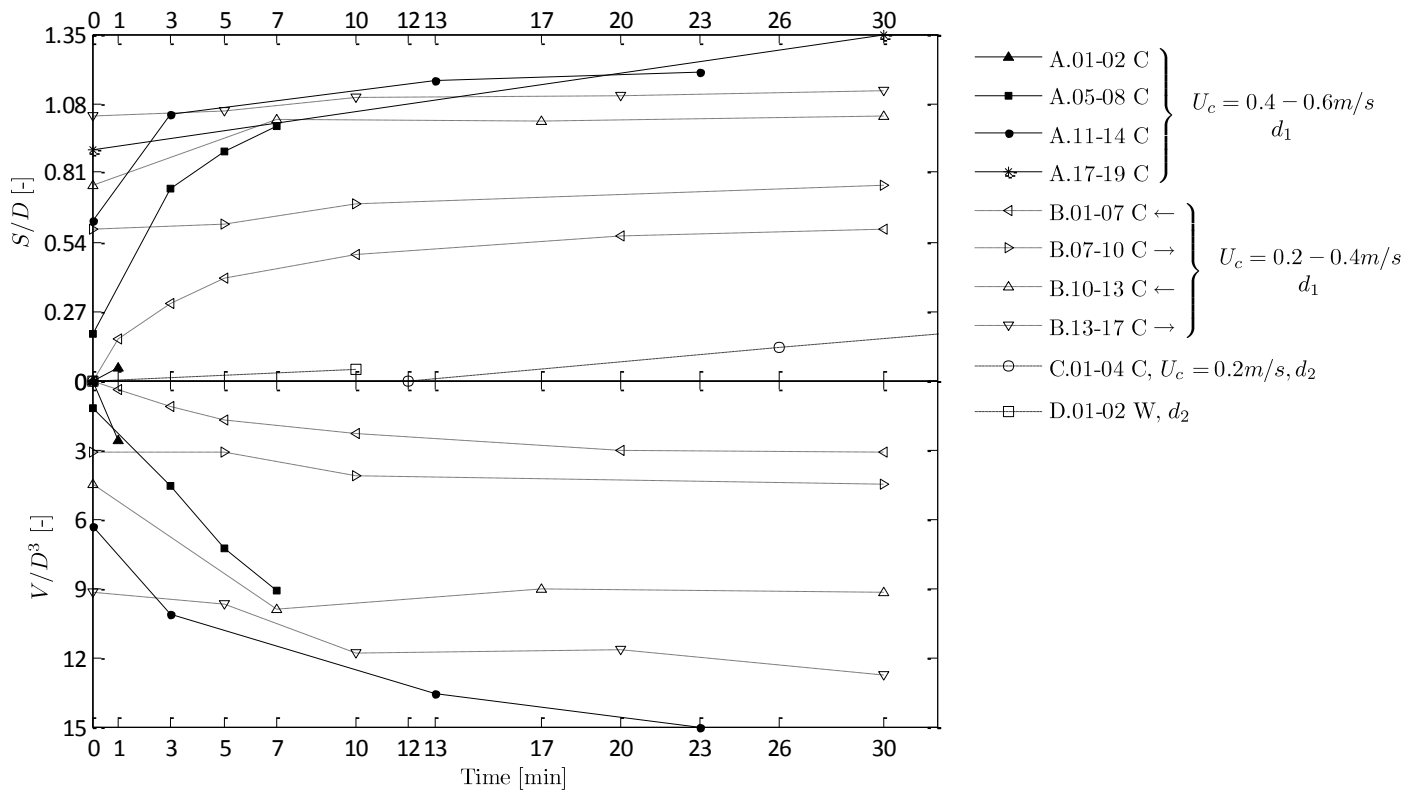
Figure 12: Measured normalized scour depth and normalized scour volume. Scour tests.
Current-only (C) or wave-only (W) flows and grain sizes $d_1 = 0.15\text{mm}$ or $d_2 = 0.10\text{mm}$.
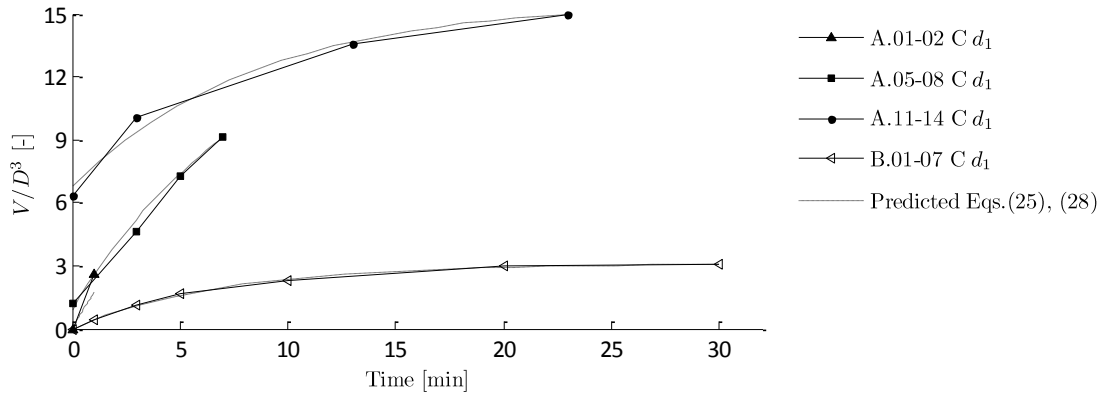
Figure 13: Measured and predicted normalized scour volume. Scour tests.
Current-only (C) flows and grain size $d_1 = 0.15\text{mm}$.
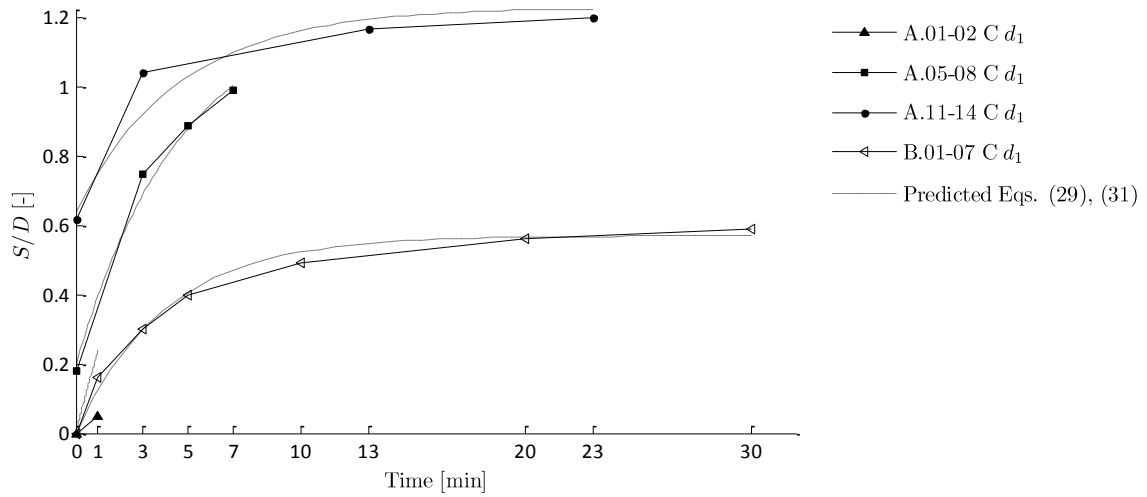
Figure 14: Measured and predicted normalized scour depth. Scour tests.
Current-only (C) flows and grain size $d_1 = 0.15\text{mm}$.
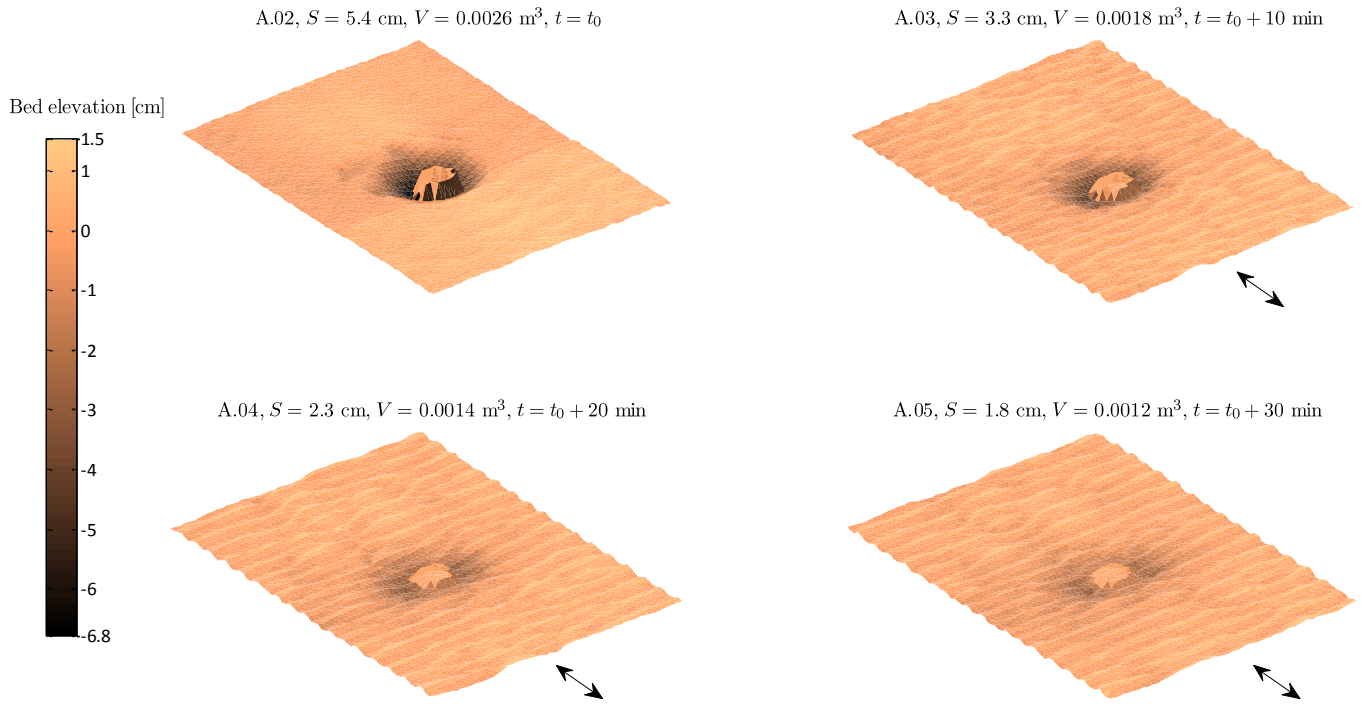
Figure 15: Bed surface development. Backfilling tests A.02-05 (Waves) with near-bed undisturbed Keulegan-Carpenter number $\kappa = 3$ and undisturbed Shields number $\theta \approx 0.2$. Double arrows indicate wave motion.

Hartvig et al. (2010) Experimental study of the development of scour & backfilling

Longitudinal section (*x* = 405 mm)
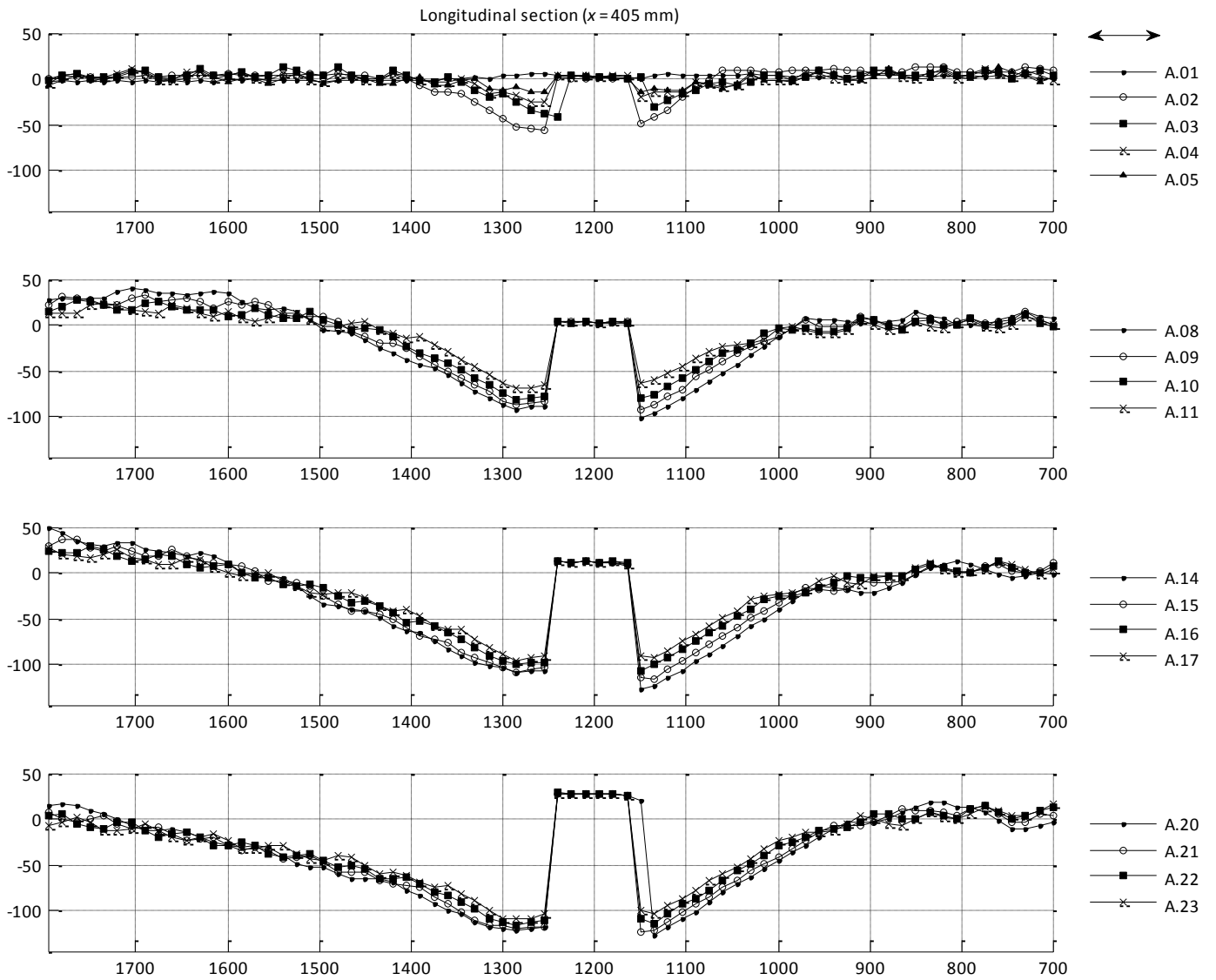
Figure 16: Longitudinal sections. Wave sequences. Series A. Bed elevation and longitudinal axis z in mm.

Hartvig et al. (2010) Experimental study of the development of scour & backfilling

Lateral section ($z = 1210$ mm)
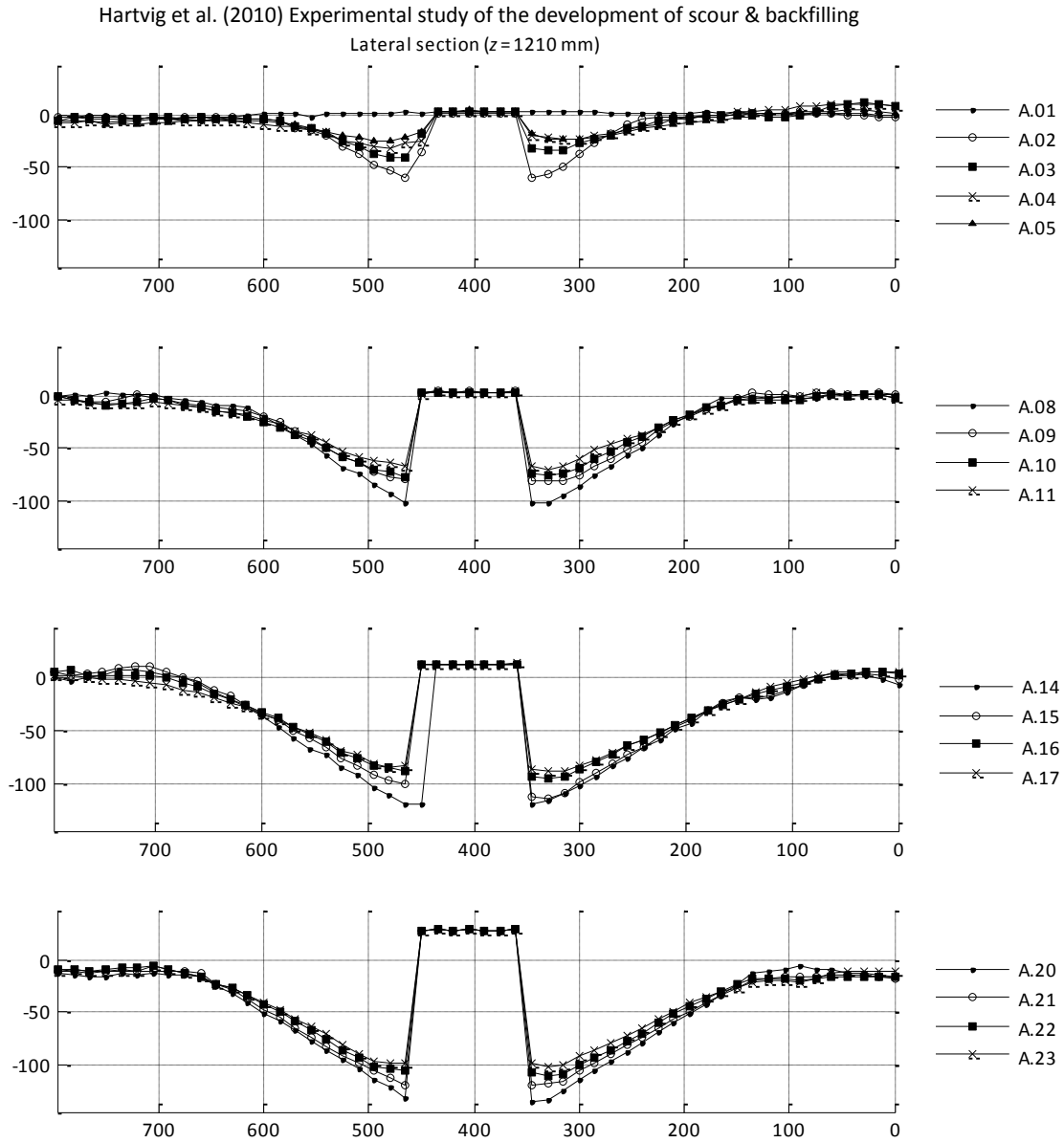
Figure 17: Lateral sections. Wave sequences. Series A. Bed elevation and lateral axis x in mm.
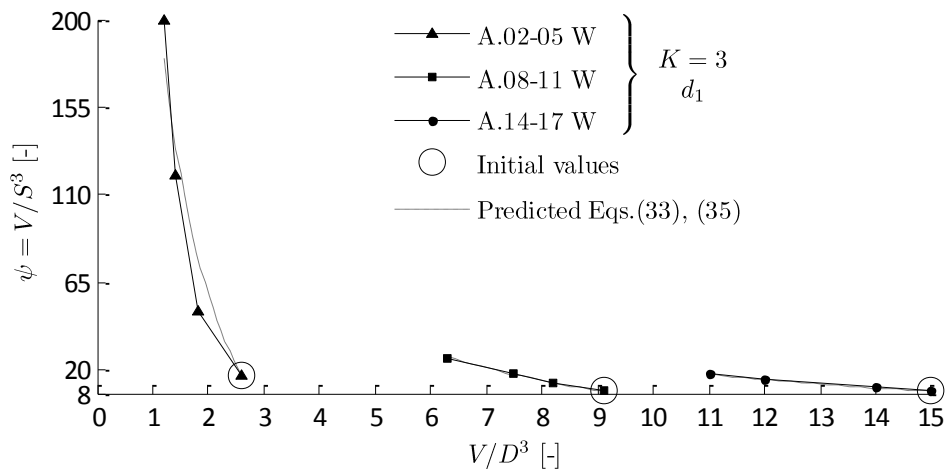
Figure 18: Scour shape factor and normalized scour volume. Measured and predicted for backfilling tests. Wave-only flows (W) and grain size $d_1 = 0.15$mm.
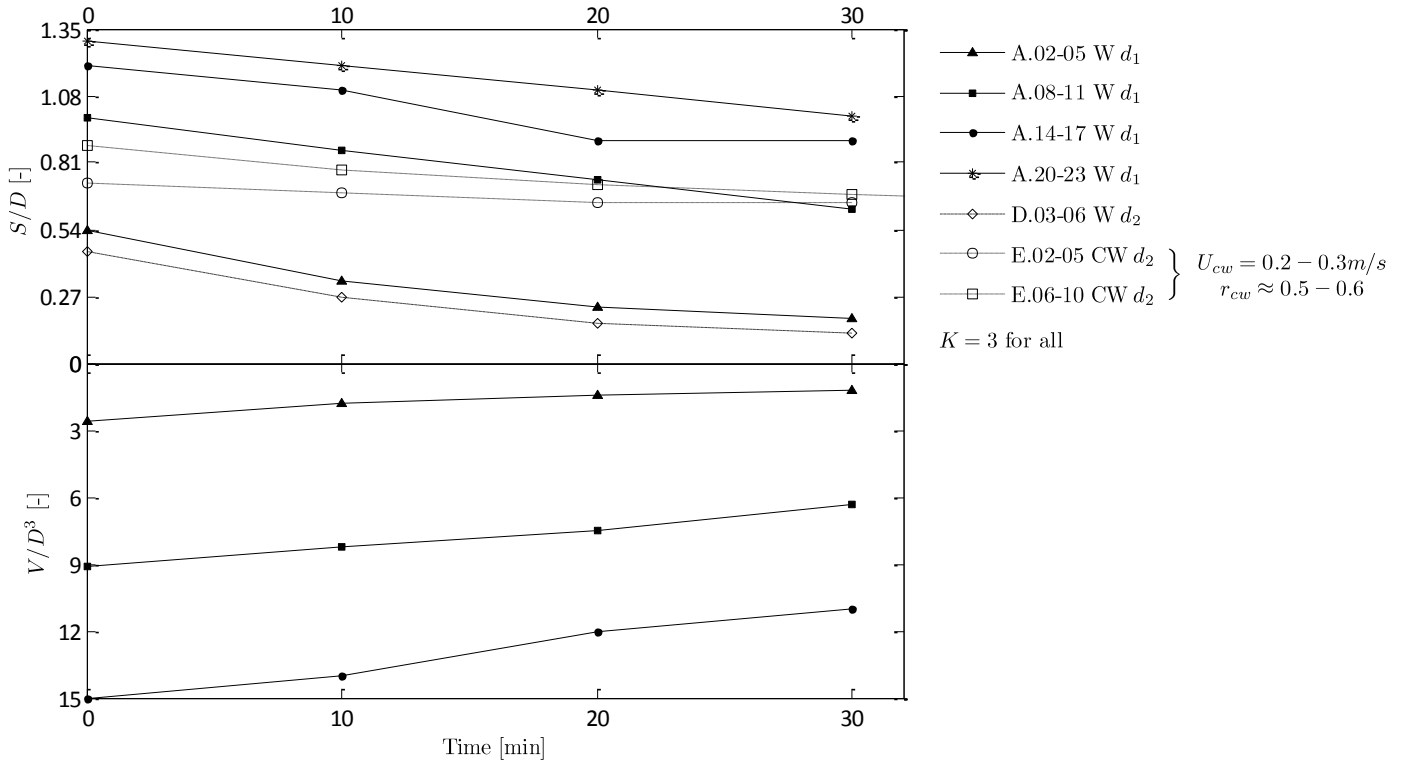
Figure 19: Normalized scour depth and normalized scour volume. Backfilling tests.
Wave-only (W) flows or combined current and waves (CW). Grain sizes $d_1 = 0.15$mm or $d_2 = 0.10$mm.

Figure 20: Measured and predicted normalized scour volume. Backfilling tests.
Wave-only (W) flows or combined current and waves (CW). Grain sizes $d_1 = 0.15$mm or $d_2 = 0.10$mm.

Figure 21: Schematics of development of scour and backfilling.

Table 2: Flow and bed conditions for series A. Reported values are denoted with *.

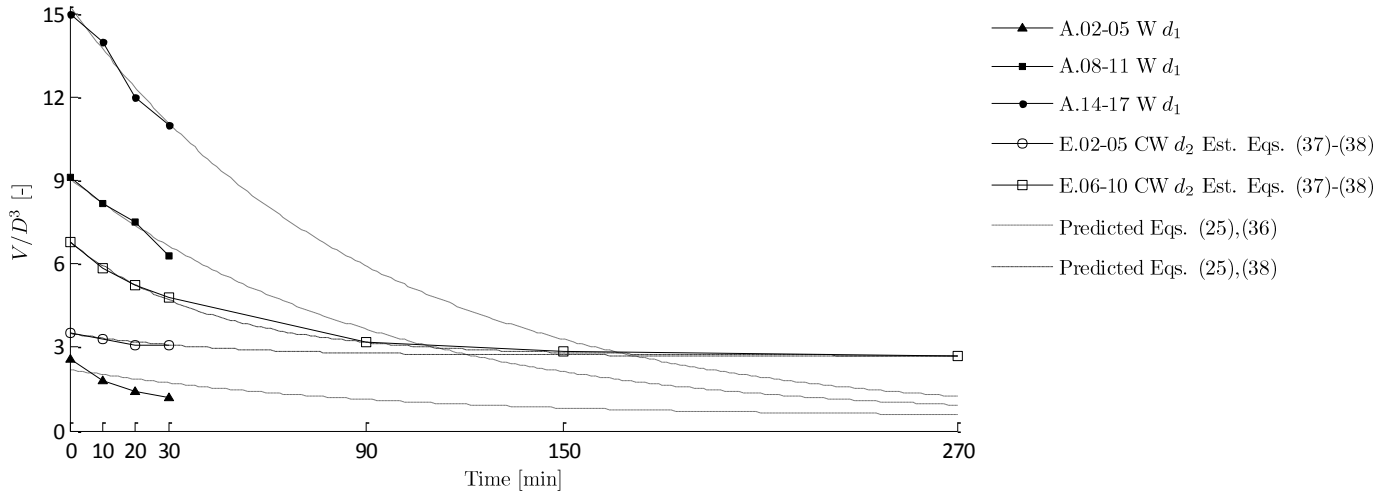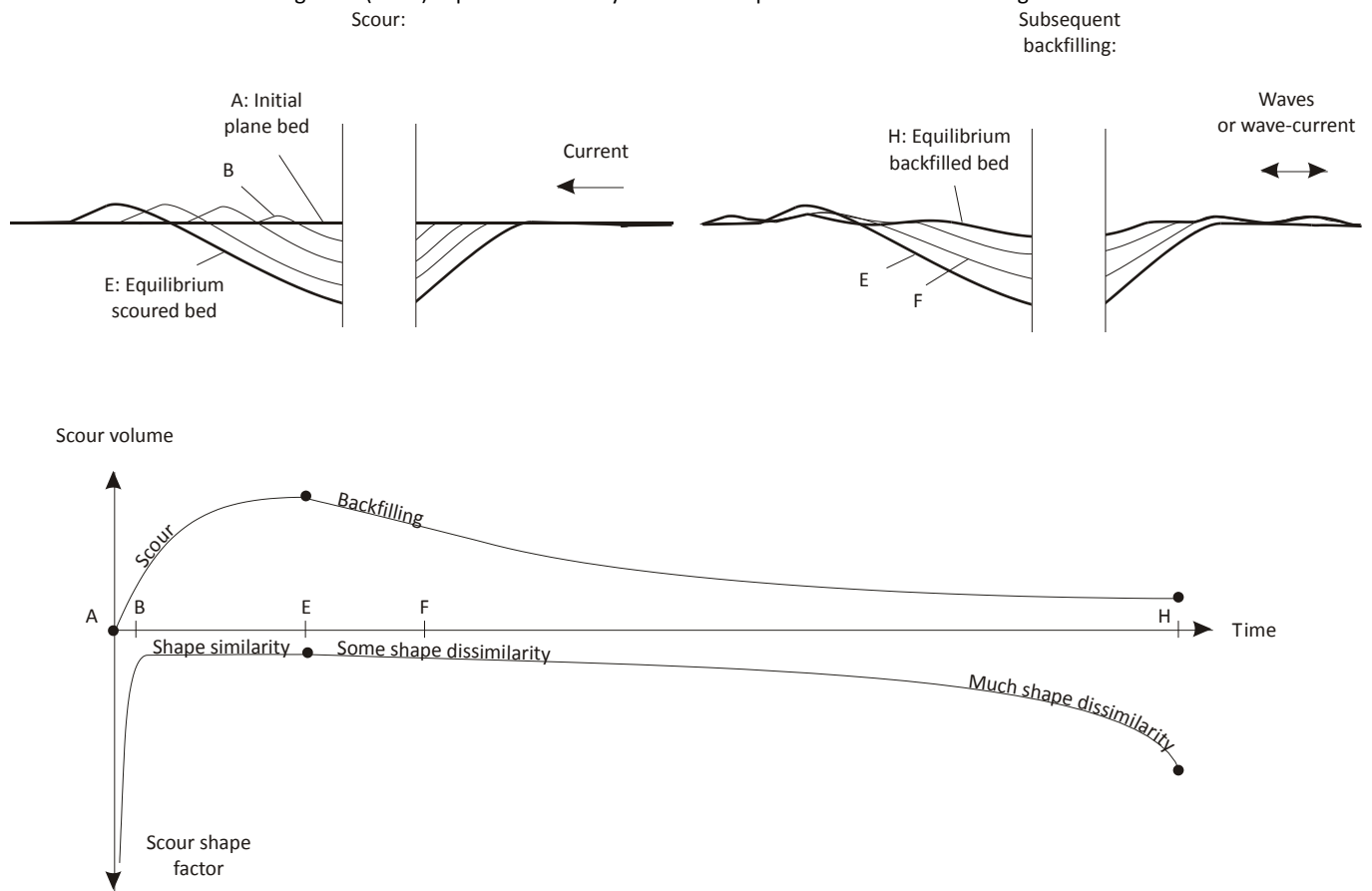|												
Series A: Current or irregular waves, live-bed scour or backfilling												
		Flow conditions				*Bed conditions*						
Profile no.	Time	Current /Waves	Mean mid-depth current velocity	Charac-teristic near-bed wave velocity	Keulegan-Carpenter no.	Global erosion	Scour depth	Scour volume	Scour shape factor	Bed wave height	Bed wave length	Shields number
	t		U_c	U_{m0}	K		S	V	ψ			θ
-	min	-	m/s	m/s	-	cm	cm	m^3	-	cm	cm	-
A.01	0	-	-	-	-	0	0	0	-	-	-	-
A.02	1	C	0.5*	-	∞	0	5.4	0.0026	17	0.5	12	0.2
A.03	11	W	-	0.2	3	0	3.3	0.0018	50	1	6	0.2
A.04	21	W	-	0.2	3	0	2.3	0.0014	120	0-1	6	0.2
A.05	31	W	-	0.2	3	0	1.8	0.0012	200	1	6	0.2
A.06	34	C	0.5	-	∞	0	7.5	0.0046	11	1	6	0.2
A.07	36	C	0.5	-	∞	0	8.9	0.0073	10	1	9	0.2
A.08	38	C	0.5	-	∞	0	9.9	0.0091	9	1	11	0.2
A.09	48	W	-	0.2	3	0	8.6	0.0082	13	1	6	0.2
A.10	58	W	-	0.2	3	0	7.4	0.0075	18	1	6	0.2
A.11	68	W	-	0.2	3	0	6.2	0.0063	26	1	6	0.2
A.12	71	C	0.4	-	∞	0	10.4	0.0101	9	1	12	0.1
A.13	81	C	0.4	-	∞	0	11.7	0.0136	9	1-2	12	0.1
A.14	91	C	0.4	-	∞	1	12	0.015	9	1-2	24	0.1
A.15	101	W	-	0.2	3	1	11	0.014	11	1	6-8	0.2
A.16	111	W	-	0.2	3	1	9	0.012	15	1	6-8	0.2
A.17	121	W	-	0.2	3	1	9	0.011	18	1	6-8	0.2
A.18	151	C	0.5	-	∞	1	13-14	0.020	8	1-3	12-17	0.2
A.19	211	C	0.5-0.6	-	∞	3	12	0.02	10	2	20	0.2-0.3
A.20	271	C	0.5*	-	∞	3	13	0.02	9	1-2	10-20	0.2
A.21	281	W	-	0.2	3	3	12	0.02	11	1	5-9	0.2
A.22	291	W	-	0.2	3	3	11	0.02	14	1	5-6	0.2
A.23	301	W	-	0.2	3	3	10	0.02	17-18	1	5-8	0.2
A.24	361	C	0.5	-	∞	4	13-15	0.03	11-12	2	15	0.2

*Table 3: Flow and bed conditions for series B. Reported values are denoted with *.*

Profile no.	Time	Current direction	Mean mid-depth current velocity	Global erosion	Scour depth	Scour volume	Scour shape factor	Bed wave height	Bed wave length	Shields number
Series B: Bidirectional current, live-bed scour										
		Flow conditions			*Bed conditions*					
	t		U_c		*S*	*V*	ψ			θ
-	min	-	m/s	cm	cm	m³	-	cm	Cm	-
B.01	0	-	-	0	0	0	-	-	-	-
B.02	1	←	0.3	0	1.6	0.0004	100	0	0	0.08
B.03	3	←	0.3	0	3.0	0.0011	40	0	0	0.08
B.04	5	←	0.4	0	4.0	0.0017	27	0	0	0.14
B.05	10	←	0.4	0	4.9	0.0023	20	0.5	6	0.14
B.06	20	←	0.3	0	5.6	0.0030	17	0.5	6	0.08
B.07	30	←	0.3	0	5.9	0.0031	15	0.5	6	0.08
B.08	35	→	0.2	0	6.1	0.0031	14	0.5-1	6	0.04
B.09	40	→	0.3	0	6.9	0.0041	12	1-2	6-10	0.08
B.10	60	→	0.3	0	7.6	0.0045	10	1-2	6-10	0.08
B.11	67	←	0.3	0	10.2	0.0099	9	1-2	10	0.08
B.12	77	←	0.3	0	10.1	0.0090	9	1-2	10	0.08
B.13	90	←	0.3	0	10.3	0.0092	8	1-2	10	0.08
B.14	95	→	0.3	0	10.5	0.0097	8	1-2	10	0.08
B.15	100	→	0.3	0	11.0	0.0118	9	1-2	10	0.08
B.16	110	→	0.3*	0	11.1	0.0117	9	1-3	10-20	0.08
B.17	120	→	0.3*	0	11.3	0.0128	9	1-3	10-20	0.08
B.18	150	←	0.3	0	11.3	0.0120	8	1-3	10-20	0.08
B.19	180	→	0.3*	0	11.9	0.0157	9	1-3	10-20	0.08

*Table 4: Flow and bed conditions for series C. Reported values are denoted with *.*
**: Although the value is zero, holes have developed away from the pile.

Profile no.	Time	Mean mid-depth current velocity	Scour depth	Shields number
Series C: Current, clear-water scour				
		Flow and bed conditions		
	t	U_c	*S*	θ
-	min	m/s	cm	-
C.01	0	-	0	-
C.02	12	0.2*	0**	0.05
C.03	26	0.2*	1.3	0.05
C.04	41	0.2*	2.5	0.05
C.05	58	0.2*	3.7	0.05
C.06	94	0.2*	4.7	0.05
C.07	134	0.2*	5.8	0.05

*Table 5: Flow and bed conditions for series D. Reported or unreported values are denoted with * or N/A, respectively.*

Series D: Current or irregular waves, live-bed scour or backfilling							
	Flow and bed conditions						
Profile no.	Time	Current /Waves	Mean mid-depth current velocity	Charac-teristic near-bed wave velocity	Keulegan-Carpenter no.	Scour depth	Shields number
-	t		U_c	U_{m0}	K	S	θ
-	min	-	m/s	m/s	-	cm	-
D.01	0	-	-	-	-	0	-
D.02	10	W	-	0.17	3	0.4	0.2
D.03	52	C	0.3*	-	∞	4.5	0.1
D.04	62	W	-	N/A	N/A	2.7	N/A
D.05	72	W	-	N/A	N/A	1.6	N/A
D.06	82	W	-	N/A	N/A	1.2	N/A

*Table 6: Flow and bed conditions for series E. Reported or unreported values are denoted with * or N/A, respectively. Dubious values are denoted with **.*

Series E: Current with irregular waves, live-bed scour or backfilling							
	Flow and bed conditions						
Profile no.	Time	Current /Waves	Mean mid-depth velocity	Charac-teristic near-bed wave velocity	Keulegan-Carpenter no.	Scour depth	Shields number
-	t		U_c, U_{cw}	U_{m0}	K	S	θ
-	min	-	m/s	m/s	-	cm	-
E.01	0	-	-	-	-	0	-
E.02	N/A	C	0.3*	-	∞	7.3	0.1
E.03	10	CW	0.3*	0.15	3	6.9	0.01**
E.04	20	CW	0.3*	N/A	N/A	6.5	N/A
E.05	30	CW	0.3*	N/A	N/A	6.5	N/A
E.06	N/A	C	0.2*	-	∞	8.8	0.05
E.07	40	CW	0.2*	0.15	3	7.8	0.01**
E.08	50	CW	0.2*	N/A	N/A	7.2	N/A
E.09	60	CW	0.2*	N/A	N/A	6.8	N/A
E.10	120	CW	0.2*	0.15	3	5.2	0.01**
E.11	180	CW	0.2*	N/A	N/A	4.9	N/A
E.12	300	CW	0.3*	N/A	N/A	4.7	N/A